PREPARATION AND PROPERTIES OF RARE-EARTH COMPOUNDS

Semiannual Technical Report
(4 January 1972 to 3 June 1972)

June 30, 1972

by

V. E. Wood, K. C. Brog, A. E. Austin, J. F. Miller
W. H. Jones, Jr., and E. W. Collings

Sponsored By

ADVANCED RESEARCH PROJECTS AGENCY

Under

ARPA Order No. 1588
PRON: W2-71-UX316-D1-DZ
Contract No. DAAHC1-70-C-1076

BATTELLE
Columbus Laboratories
505 King Avenue
Columbus, Ohio 43201

UNCLASSIFIED

Security Classification

DOCUMENT CONTROL DATA - R & D

(Security classification of title, body of abstract and indexing annotation must be entered when the overall report is classified)

1 ORIGINATING ACTIVITY (Corporate author)	2a. REPORT SECURITY CLASSIFICATION
Battelle-Columbus Laboratories 505 King Avenue Columbus, Ohio 43201	UNCLASSIFIED 2b. GROUP

3 REPORT TITLE

PREPARATION AND PROPERTIES OF RARE-EARTH COMPOUNDS

4. DESCRIPTIVE NOTES (Type of report and inclusive dates)

Semi-Annual Technical Report (3 January 1972 to 4 June 1972)

5 AUTHOR(S) (First name, middle initial, last name)

Van E. Wood, Kenneth C. Brog, Alfred E. Austin, James F. Miller, William H. Jones, Jr. and Edward W. Collings

6 REPORT DATE	7a. TOTAL NO OF PAGES	7b. NO OF REFS
June 30, 1972	47	39

8a. CONTRACT OR GRANT NO	9a. ORIGINATOR'S REPORT NUMBER(S)
DAAH01-70-C-1076 b. PROJECT NO	Battelle Project # G-0550
c.	9b OTHER REPORT NO(S) (Any other numbers that may be assigned this report)
d.	

10 DISTRIBUTION STATEMENT

Distribution of this document is unlimited

11 SUPPLEMENTARY NOTES	12 SPONSORING MILITARY ACTIVITY
	Advanced Research Projects Agency Arlington, Virginia 22209

13 ABSTRACT

The preparation and characterization and certain physical properties of some rare-earth compounds of technological potential are described. Magneto-ferroelectric materials and narrow-band narrow-gap semiconductors were investigated. In the former area, development of a simultaneously ferroelectric and ferromagnetic device element operating in a useful temperature range is the primary goal. The principal materials studied during the past six months are bismuth-neodymium ferrites. It was found that addition of neodymium led to weak ferromagnetism at room temperature in the ferroelectric $BiFeO_3$ phase. The presence of ferroelectricity in our samples has not yet been explicitly shown, however. The principal difficulties with these materials - the small magnetic moment and the high electric coercive field - can be relieved, it is anticipated, by improved preparation techniques and further alloying additions. Narrow-band narrow-gap semiconductors undergoing purely electronic semiconductor-to-metal transitions are of considerable interest. In the past six months, a nuclear-magnetic-resonance study of certain samarium monochalcogenides, which undergo semiconductor-to-metal transitions at elevated pressure, was carried out in order to determine the degree of localization of the samarium 4f states in these materials. Experiments on cathodoluminescence in these materials and further investigations of allegedly ferroelectric ytterbium chromite are also reported briefly.

DD FORM 1 NOV 65 1473

UNCLASSIFIED

Security Classification

14 KEY WORDS	LINK A		LINK B		LINK C	
	ROLE	WT	ROLE	WT	ROLE	WT
Magnetoferroelectric Materials						
Semiconducting Compounds						
Semiconductor-to-metal transitions						
Cathodoluminescence						
Rare-earth chalcogenides						
Rare-earth ferrites						
Bismuth ferrite						

PREPARATION AND PROPERTIES OF RARE-EARTH COMPOUNDS

Semiannual Technical Report
(4 January 1971 to 3 June 1972)

June 30 1972

by

V. E. Wood, K. C. Brog, A. E. Austin, J. F. Miller
W. H. Jones, Jr., and E. W. Collings

Sponsored By

ADVANCED RESEARCH PROJECTS AGENCY

Under

ARPA Order No. 1588
PRON: W2-71-UX316-D1-DZ
Contract No. DAAH01-70-C-1076
(Modif. P00003, 4 June 1971 - 3 June 1972, $199,000)

Project Technical Director: V. E. Wood
Phone Number: (614) 299-3151, Ext. 2780

Monitored by: ARPA Support Office
U. S. Army Missile Command (AMSMI-RND)
Redstone Arsenal, Alabama

BATTELLE
Columbus Laboratories
505 King Avenue
Columbus, Ohio 43201

SUMMARY

The preparation and characterization and certain physical properties of some rare-earth compounds of technological potential are described. Magneto-ferroelectric materials and narrow-band narrow-gap semiconductors were investigated. In the former area, development of a simultaneously ferroelectric and ferromagnetic device element operating in a useful temperature range is the primary goal. The principal materials studied during the past six months are bismuth-neodymium ferrites. It was found that addition of neodymium led to weak ferromagnetism at room temperature in the ferroelectric $BiFeO_3$ phase. The presence of ferroelectricity in our samples has not yet been explicitly shown, however. The principal difficulties with these materials - the small magnetic moment and the high electric coercive field - can be relieved, it is anticipated, by improved preparation techniques and further alloying additions. Narrow-band narrow-gap semiconductors undergoing purely electronic semiconductor-to-metal transitions are of considerable interest. In the past six months, a nuclear-magnetic-resonance study of certain samarium monochalcogenides, which undergo semiconductor-to-metal transitions at elevated pressure, was carried out in order to determine the degree of localization of the samarium 4f states in these materials. Experiments on cathodoluminescence in these materials and further investigations of allegedly ferroelectric ytterbium chromite are also reported briefly.

TABLE OF CONTENTS

LIST OF TABLES

LIST OF FIGURES

LIST OF FIGURES (Cont'd)

INTRODUCTION

The aim of this program is development of the device potential of rare-earth compounds having unusual and previously unexploited physical properties. Two properties, or types of properties, are being studied. The first is the simultaneous occurence of ferromagnetic and ferroelectric ordering, or more generally, the dielectric properties of magnetically-ordered materials and the interactions between the electric and magnetic moments. These effects might be used in a number of signal-modification applications in semiconducting materials, and in memory and switching applications in transparent materials. The second type of property is the semiconductor-to-metal transition found in certain narrow-band semiconductors which might find application in fast, reliable switching and in overload-protection devices. These properties have not been used much so far principally because of the lack of really suitable materials; our work has therefore emphasized development of such materials.

The present report describes only the work of the past six months. Further background on the phenomena being studied can be found in our report of 30 June, 1971 (AD 726 201). A summary of the accomplishments of the entire program will be included in the Final Report on this project to be submitted at the end of 1972. The two areas of investigation, magnetoelectric materials and narrow-band semiconductors, will be discussed in turn.

MAGNETOELECTRIC MATERIALS

The aim of this work is the development of a material which is both ferromagnetic and ferroelectric in a useful temperature range. Such a material should have unique memory or signal-processing capabilities. We believe we have recently found some room-temperature ferroelectric ferromagnets in the $Bi_{1-x}Nd_xFeO_3$ system, although some further verification is necessary and considerable development may be required before these or similar materials find actual application. This is discussed briefly in the introductory remarks to the following subsection, which summarizes our work to date on this system. Previously, we had studied for the most part rare-earth manganites and their solid solutions with chromites and ferrites. Some of that work has continued during the past six months and is discussed briefly in the second subsection of this section.

Bismuth-neodymium ferrites

There have been numerous experiments reported in the Russian literature on inducing a weak magnetic moment in otherwise antiferromagnetic, and ferroelectric, $BiFeO_3$ by partial replacement of the bismuth by a rare earth. Neodymium, the most attractive ion from the standpoint of ionic size and unique valency, had not, however, been tried. Upon preparing a number of solid solutions in the $Bi_{1-x}Nd_xFeO_3$ system, we found that $Bi_{.9}Nd_{.1}FeO_3$, which retains the rhombohedral, and presumably ferroelectric, structure of $BiFeO_3$ had a small magnetic moment at room temperature. $Bi_{.85}Nd_{.15}FeO_3$, which has a possibly ferroelectric tetragonal structure different from that of either end member, has a slightly larger moment. Attempts to detect ferroelectricity, or any acentric property which could be studied through the ferroelectric ordering temperature, have not so far been successful in these solid-solution samples. Piezoelectricity

was detected, however, in a sample of undoped $BiFeO_3$ grown from flux in a thick-walled nickel crucible, and it is expected that further flux-growth experiments will produce solid-solution samples in which ferroelectric properties can be studied.

As things now stand, bismuth-neodymium ferrites present several disadvantages from the potential device standpoint:

1) the conductivity seems to be somewhat high, although this has not yet been directly determined,
2) the electric coercive field is extremely high, leading to the formation of multidomain ferroelectric samples despite the high conductivity,
3) the magnetic moment is somewhat small and dependent on thermal history.

There is no doubt that all these disadvantages can be relieved by a combination of modified preparation procedures and further alloying additions, but the extent to which this can be done remains to be seen.

In the following paragraphs, the preparation, crystallography, and magnetic properties of the bismuth-neodymium ferrites are discussed in turn.

Materials Preparation

The investigation of solid solutions between ferroelectric $BiFeO_3$ and weakly ferromagnetic $(RE)FeO_3$ compounds was initiated toward the end of the previous semiannual report period with work on the $Bi_{1-x}Nd_xFeO_3$ system. Preparative work on this system has continued through this semiannual period, utilizing three general approaches to the preparation of the materials: (1) solid-state reaction of intimate mixtures of oxides prepared by coprecipitation of the hydroxides, (2) solid-state reaction of physical mixtures of oxides containing excess Bi_2O_3,[1] and (3) reaction and crystallization from solution in excess

Bi_2O_3 flux. Stoichiometric solid-solution specimens were obtained by use of the solid-state reaction and flux methods; the coprecipitation method yielded specimens of a new Bi_2O_3- deficient tetragonal phrase.

For all of these preparations, starting materials were reagent grade Bi_2O_3, 99.9% pure Nd_2O_3, and 99.999% pure $FeCl_2$. The high-purity iron compound was employed to minimize the concentrations of strongly ferromagnetic transition-metal impurities that typically are present. Since strongly magnetic impurities generally are not present in bismuth and neodymium oxides, purity of these materials was not considered to be as critical; so readily available CP grades were used.

Coprecipitation In initial preparations, the coprecipitation technique was used with the objective of obtaining intimate stoichiometric mixtures of the constituents. Stoichiometric proportions of the constituent elements were taken into solution in dilute acid. The acid solution then was rapidly neutralized with a 100% excess of ammonium hydroxide solution, thus precipitating an intimate mixture of hydroxides. After thorough washing, the mixtures were fired to dehydrate the material and to carry out the solid-state reaction. The final firing temperatures generally were held below the reported decomposition temperature of $BiFeO_3$[2,3] at 750-780 C. In these preparations, as well as in subsequent ones by the other techniques, all high-temperature reactions were carried out in oxygen atmospheres.

As can be seen from data on the preparations employing coprecipitation, which are summarized in the first portion of Table 1, this preparation did not yield materials with the expected rhombohedral ($BiFeO_3$) or orthorhombic (RE orthoferrite) structures, even though prolonged reaction times (e.g., as in

TABLE 1. SUMMARY OF SELECTED EXPERIMENTS ON PREPARATION OF $Bi_{1-x}Nd_xFeO_3$

Preparation Number	Nominal Composition	Excess Bi_2O_3, %	Firing Conditions: Form[a]	Temperature, °C	Time, hr	Post-Firing[b] Treatment	Phases Detected[c]
			Coprecipitations				
28886-75	$BiFeO_3$	--	Powder	780	24		
			Pellet	780	49	None	$Bi_2Fe_4O_9$, Bi_2O_3
28886-76	$Bi_{0.85}Nd_{0.15}FeO_3$	--	Powder	780	24		
			Pellet	780	49	None	New tetragonal phase (c/a = 2.3), tr Bi_2O_3, tr α Fe_2O_3
28886-87	$BiFeO_3$ (-75 re-ground)	--	Powder	750	24		
			Pellet	750	48	None	$Bi_2Fe_4O_9$
28886-83	$BiFeO_3$	--	Pellet	750	72	"	$Bi_2Fe_4O_9$
28886-84A	$Bi_{0.5}Nd_{0.5}FeO_3$	--	Powder	750	24		New tetragonal phase
28886-84B	$Bi_{0.5}Nd_{0.5}FeO_3$	100	Powder	750	8	Acid leached	α Fe_2O_3
28886-85A	$Bi_{0.75}Nd_{0.25}FeO_3$	--	Powder	750	24		
			Pellet	750	48		New tetragonal phase
28886-85B	(-85A processed further)	--	Pellet	900	48		New tetragonal phase
28886-86A	$Bi_{0.65}Nd_{0.35}FeO_3$	--	Powder	750	24		New tetragonal phase
28886-86B	$Bi_{0.65}Nd_{0.35}FeO_3$	100	Powder	750	8	Acid leached	α Fe_2O_3
28886-88	$Bi_{0.85}Nd_{0.15}FeO_3$ (-76 reground)	--	Pellet	900	48		Desired tetragonal phase (c/a = 1.39), tr new tetragonal phase, tr Bi_2O_3
			Solid-State Reactions				
28886-92	$BiFeO_3$	100	Powder	750	6	Acid leached	Rhombohedral $BiFeO_3$
28886-96A	$Bi_{0.85}Nd_{0.15}FeO_3$	100	Powder	750	16	Ditto	Desired tetragonal phase
28886-96B	(-96A processed further)[d]	--	Powder	900	24	"	Desired tetragonal phase, tr $Bi_2Fe_4O_9$ phase
28886-97A	$Bi_{0.75}Nd_{0.25}FeO_3$	100	Powder	750	8		Orthorhombic (RF orthoferrite) phase
28886-97B	(-97A processed further)[d]	--	Powder	900	24		Orthorhombic phase, tr $Bi_2Fe_4O_9$ phase
29528-1	$Bi_{0.5}Nd_{0.5}FeO_3$	10	Powder	1200	24		Orthorhombic phase
29528-2	$Bi_{0.65}Nd_{0.35}FeO_3$	10	Powder	1075	24	"	Orthorhombic phase
29528-3A	$Bi_{0.8}Nd_{0.2}FeO_3$	100	Powder	750	16	"	$Bi_2Fe_4O_9$ phase, minor α Fe_2O_3 phase
29528-3B	(-3A processed further)[d]	--	Powder	900	24		Orthorhombic phase, tr $Bi_2Fe_4O_9$ phase
29528-11	$Bi_{0.9}Nd_{0.1}FeO_3$	10	Pellet	750	144	"	$Bi_2Fe_4O_9$ phase
29528-12	$Bi_{0.95}Nd_{0.05}FeO_3$	10	Pellet	750	144	"	$Bi_2Fe_4O_9$ phase
29528-17	$Bi_{0.9}Nd_{0.1}FeO_3$	100	Powder	725	16		$Bi_2Fe_4O_9$ phase, α Fe_2O_3, minor perovskite phase
29528-18	$Bi_{0.95}Nd_{0.05}FeO_3$	100	Powder	725	16	"	$Bi_2Fe_4O_9$ phase, α Fe_2O_3, minor perovskite phase
29528-21	$Bi_{0.9}Nd_{0.1}FeO_3$	100	Powder	850	16	"	Desired rhombohedral solid-solution phase, tr $Bi_2Fe_4O_9$ phase
29528-22	$Bi_{0.95}Nd_{0.05}FeO_3$	100	Powder	850	16		Desired rhombohedral solid-solution phase
29528-23	$Bi_{0.9}Nd_{0.1}FeO_3$	100	Powder	725	96	"	$Bi_2Fe_4O_9$ phase mainly
29528-24	$Bi_{0.95}Nd_{0.05}FeO_3$	100	Powder	725	96	"	$Bi_2Fe_4O_9$ phase mainly
			Flux Growths				
29528-10	$BiFeO_3$	~400	Temp 850° → 515° at 2.9° hr			Acid leached	Rhombohedral $BiFeO_3$
29528-16	$Bi_{0.95}Nd_{0.05}FeO_3$	~400	Temp 875 → 515° at 2.9°/hr				Sound ($NiFe_2O_4$)

(a) Material in powder form was packed by hand-pressure into a platinum container. Pellets were prepared by cold pressing in steel dies at about 80,000 psi.

(b) The acid-leaching step involved grinding the material in four successive baths of concentrated nitric acid to dissolve excess Bi_2O_3, then washing similarly three times and finally washing on a filter with deionized water.

(c) Phase analysis of the polycrystalline material was done by X-ray diffraction. Powder patterns were taken in 57.3-mm diameter cameras with Fe K α radiation. tr indicates a trace was detected.

(d) Before acid leaching.

preparation -83) and higher reaction temperatures (e.g., preparations -85B and -88) were employed. Howeve a new tetragonal structure, with c/a = 2.3, was seen in a number of the solid-solution materials. Chemical analysis of two samples, from preparations 28886-83 and 28886-85, showed that these materials are Bi_2O_3 deficient, by 2 and 3.5 weight percent, respectively. It is concluded that bismuth was not quantitatively precipitated by the ammonium hydroxide, and that a previously unreported tetragonal phase is obtained from Bi_2O_3-deficient charges.

Solid-State Reactions The desired perovskite and solid-solution materials were prepared by solid-state reactions of Bi_2O_3-rich mixtures of oxides similar to those of Achenbach et al[1] for $BiFeO_3$. Roginskaya et al[4] and Viskov et al[5] reported making similar solid solutions by sintering stoichiometric mixtures of the oxides. In our preparations, the oxide mixtures were fired in oxygen atmospheres at the selected temperatures for various lengths of time. Multiple firings, intermediate grinding, and cold pressing of the material were employed to maximize contact and promote reaction and homogenization. Following the solid-state reaction, the excess Bi_2O_3 was removed by multiple leaching of the material (by grinding) in concentrated nitric acid, and thorough, multiple washing.

As can be seen from the data summarized in Table 1 on the solid-state reactions, results are in general agreement with those reported by others for the preparation of $BiFeO_3$ and $BiFeO_3$-(RE)FeO_3 solid solutions. Single-phase $BiFeO_3$ and solid-solution materials can be obtained by relatively short-term reaction of the Bi_2O_3-rich oxide mixtures (as in preparations -92 and -97A, for example). A reaction temperature of about 750 C appears satisfactory for the synthesis of $BiFeO_3$, while higher temperatures are required for solid-solution

synthesis as the Nd_2O_3 content increases (e.g., preparations -1 and -2). If high reaction temperatures are used, disproportionation to $Bi_2Fe_4O_9$ and Bi_2O_3 appears to occur (as in preparation -96B vs. -96A, - 97B vs. -97A) in accord with indications of the Bi_2O_3 - Fe_2O_3 phase diagram.

However, results were not entirely consistent. In some preparations (not tabulated) the desired phase failed to form after prolonged and repeated reaction. This inconsistency is tentatively attributed to differences between reactivities of the several lots of Fe_2O_3 that were used. In some cases (e.g., preparations -21 and -22) the reaction appeared to go only when the temperature was raised above the melting point of Bi_2O_3.

The results are summarized schematically in Figure 1, along with those for some of the coprecipitation syntheses. As is indicated, the expected perovskite and solid-solution structures were obtained only from Bi_2O_3-rich starting materials, while Bi_2O_3-deficient (coprecipitated) charges yielded material with a new tetragonal structure. Solid-solutions with the rhombohedral $BiFeO_3$ structure were prepared which contained 5 and 10 mole percent $NdFeO_3$. Material containing 15 mole percent $NdFeO_3$ had a tetragonal structure, c/a = 1.39, while samples containing 20, 25, 35, and 50 mole percent $NdFeO_3$ had the orthorhombic (orthoferrite) structure.

Flux Growth Several preliminary experiments, which also are summarized at the bottom of Table 1, have been conducted on the growth of $Bi_{1-x}Nd_xFeO_3$ crystals from Bi_2O_3 flux. Nickel crucibles, as suggested by Gerson et al,[6] were employed, and selection of the Bi_2O_3 concentration (400% excess) was based on the phase-diagram data. Although $BiFeO_3$ was obtained in the first of these runs (preparation -10), the material was found by optical-emission spectrographic analysis to contain 0.1 weight percent nickel. In the following preparation, -16,

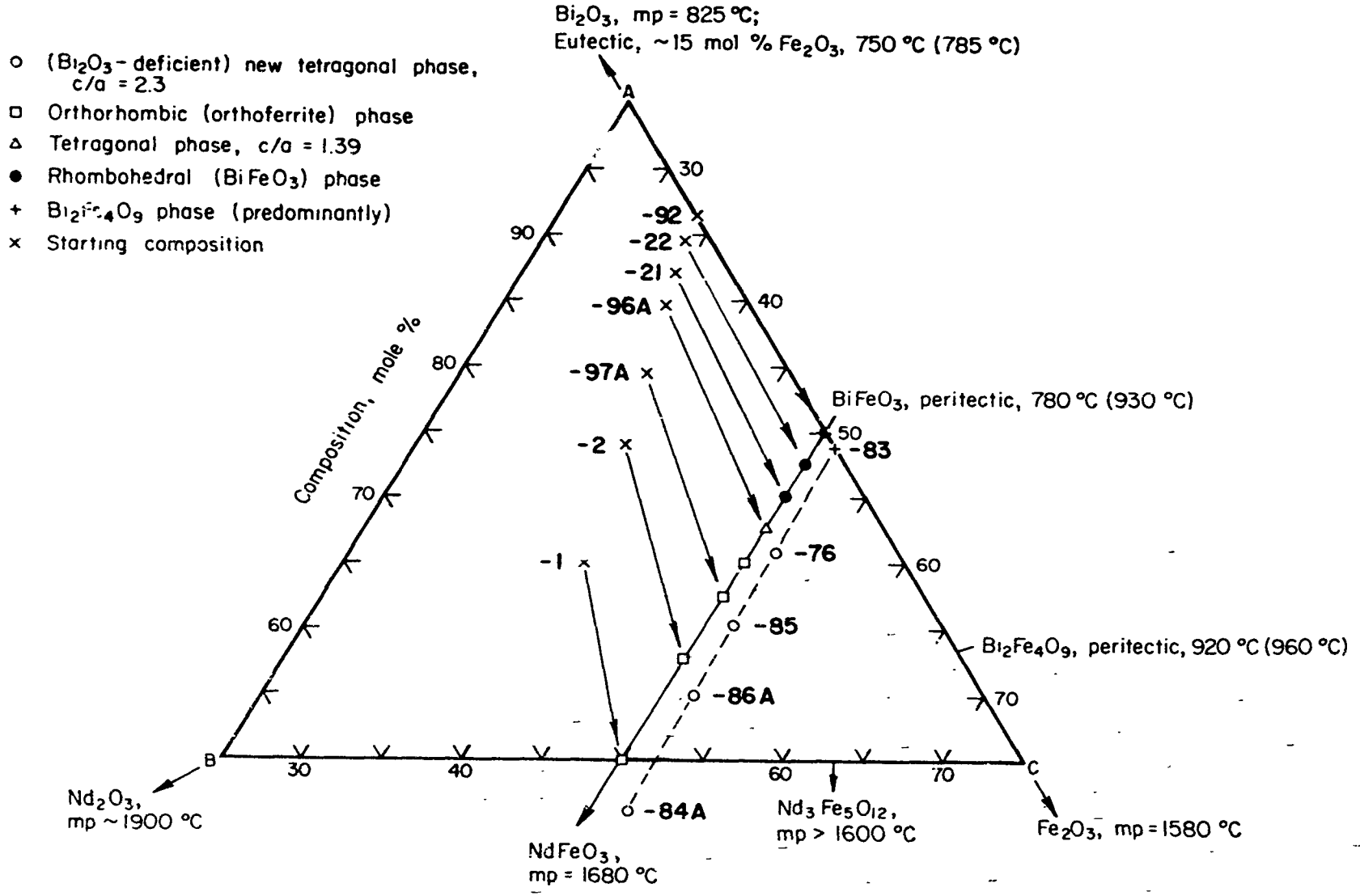

FIGURE 1

Portion of the Bi_2O_3-Nd_2O_3-Fe_2O_3 phase diagram. Liquidus temperatures of eutectic and peritectic compositions given in parentheses. Heavy numbers are sample numbers of Table I.

aimed at growth of solid-solution crystals, the nickel crucible was attacked severely and the product principally was a spinel phase—probably $NiFe_2O_4$. In subsequent experiments on single-crystal synthesis, other container materials, such as the Pt-group metals, will have to be investigated.

Crystallography of $Bi_{1-x}Nd_xFeO_3$

The end phases in the system $Bi_{1-x}Nd_xFeO_3$ are rhombohedral $BiFeO_3$ and orthorhombic $NdFeO_3$. Both phases are distortions of the cubic perovskite structure. Prior studies of $BiFeO_3$-$PrFeO_3$[5] and $BiFeO_3$-$LaFeO_3$[4] had shown limited solid solutions in $BiFeO_3$ and extensive solid solution in the rare-earth ferrite. An intermediate tetragonal phase $Bi_{1-x}Pr_xFeO_3$, for $0.2 < x < 0.3$, was reported to be weakly ferromagnetic and simultaneously ferroelectric. In contrast, the comparable region in $Bi_{1-x}La_xFeO_3$ was claimed to be weakly ferromagnetic but antiferroelectric. The system $BiFeO_3$-$NdFeO_3$ was chosen for seeking a solid solution phase with magneto ferroelectric properties. Neodymium was selected on the basis that its ionic radius of 1.12Å was close to that of 1.11Å for bismuth and that it had but one stable oxidation state of +3. In the system $BiFeO_3$-$PrFeO_3$ there is the possibility of variable oxidation state of +2, +3, and +4 for praseodymium and thus a mixture of +2 and +3 for the iron as the cause of weak ferromagnetism. The variable oxidation states for the cations could also increase the electrical conductivity. $BiFeO_3$ has a rhombohedral structure in space group R3c with two formula units in the unit cell.[6] It is ferroelectric and antiferromagnetic with magnetic cell coinciding with the crystallo-chemical cell.[7,8] Its Neel temperature is 365 C and its ferroelectric Curie temperature is greater than its decomposition temperature of 780 C. The space group R3c permits ferromagnetism with magnetic group R3c'. With this magnetic symmetry, the net magnetic moment must be along the three-fold axis, and thus parallel to the polarization

of the ferroelectric state. The antiferromagnetic structure is of the G type with Fe^{3+} spins perpendicular to the three-fold axis, i.e., in the basal plane. For the incidence of weak ferromagnetism, the Fe^{3+} spins would need to be deflected a small amount from the basal plane to give a component along the three-fold axis. In $BiFeO_3$ there are small displacements of the cations from ideal cubic positions along the trigonal axis and slight rotations of the oxygen octahedra.[6]

The cation and oxygen ion displacements result in considerable variation in Bi-O distances for the nominal 12-fold coordination. Of the 12 Bi-O distances 3 have a length of 2.30Å, another 3 a length of 2.52Å and the remaining 6 have lengths varying from 3.14 to 3.38Å; these are to be compared to 2.79Å for ideal cubic perovskite. The six Fe-O distances are 1.95 to 2.11Å instead of the ideal 2.01Å. The magnitude of the off-center displacement of the Fe^{3+} relative to its oxygen octahedra indicates a ferroelectric Curie temperature of about 840 ± 50 C and a spontaneous polarization of 60 $\mu C/cm^2$ according to the relationship for displacive ferroelectrics.[9] The high Curie temperature and large polarization with high electric-coercivity field place $BiFeO_3$ in the class of "hard" ferroelectrics.

$NdFeO_3$ has an orthorhombic structure, space group Pbnm, with four formula units in the unit cell. It is a weak ferromagnet with a Neel temperature of 415 C. The iron sublattice has spin order F_z, with the weak net moment along the c-axis.[10]

Along the pseudo-binary $Bi_{1-x}Nd_xFeO_3$, three solid-solution phases exist at room temperature. These are rhombohedral $BiFeO_3$ for $0 < x < 0.1$, a tetragonal phase for $Bi_{.85}Nd_{.15}FeO_3$, and the orthorhombic orthoferrite phase for $0.2 < x < 1.0$. Table 2 lists the unit cell parameters and molar volumes, Ω, and Figure 2 shows the variation with x for $Bi_{1-x}Nd_xFeO_3$. In the rhombohedral

TABLE 2. CRYSTAL STRUCTURE DATA ON $Bi_{1-x}Nd_xFeO_3$

	Unit Cell Parameters* and Molar Volume						
	Rhombohedral			Orthorhombic			
Composition	a_R	α	Ω	a_o	b_o	c_o	Ω
$BiFeO_3$	5.638	59°18'	62.3	-	-	-	-
$Bi_{.95}Nd_{.05}FeO_3$	5.631	59°18'	62.1	-	-	-	-
$Bi_{.9}Nd_{.1}FeO_3$	5.624	59°22'	62.0	-	-	-	-
$Bi_{.85}Nd_{.15}FeO_3$	-	-	-	5.60	5.60	7.80	61.2
$Bi_{.80}Nd_{.20}FeO_3$	-	-	-	5.43	5.59	7.90	59.9
$Bi_{.75}Nd_{.25}FeO_3$	-	-	-	5.43	5.57	7.90	59.7
$Bi_{.65}Nd_{.35}FeO_3$	-	-	-	5.44	5.59	7.80	59.3
$Bi_{.5}Nd_{.5}FeO_3$	-	-	-	5.42	5.58	7.80	60.0
$NdFeO_3$ (a)	-	-	-	5.441	5.573	7.753	58.8

* a_o, b_o, c_o unit cell parameters in Angstroms, error ± 0.005 A

Ω = volume per formula unit (A^3)

(a) Geller, S., and Wood, E. A., Acta Cryst. 9, 563 (1956).

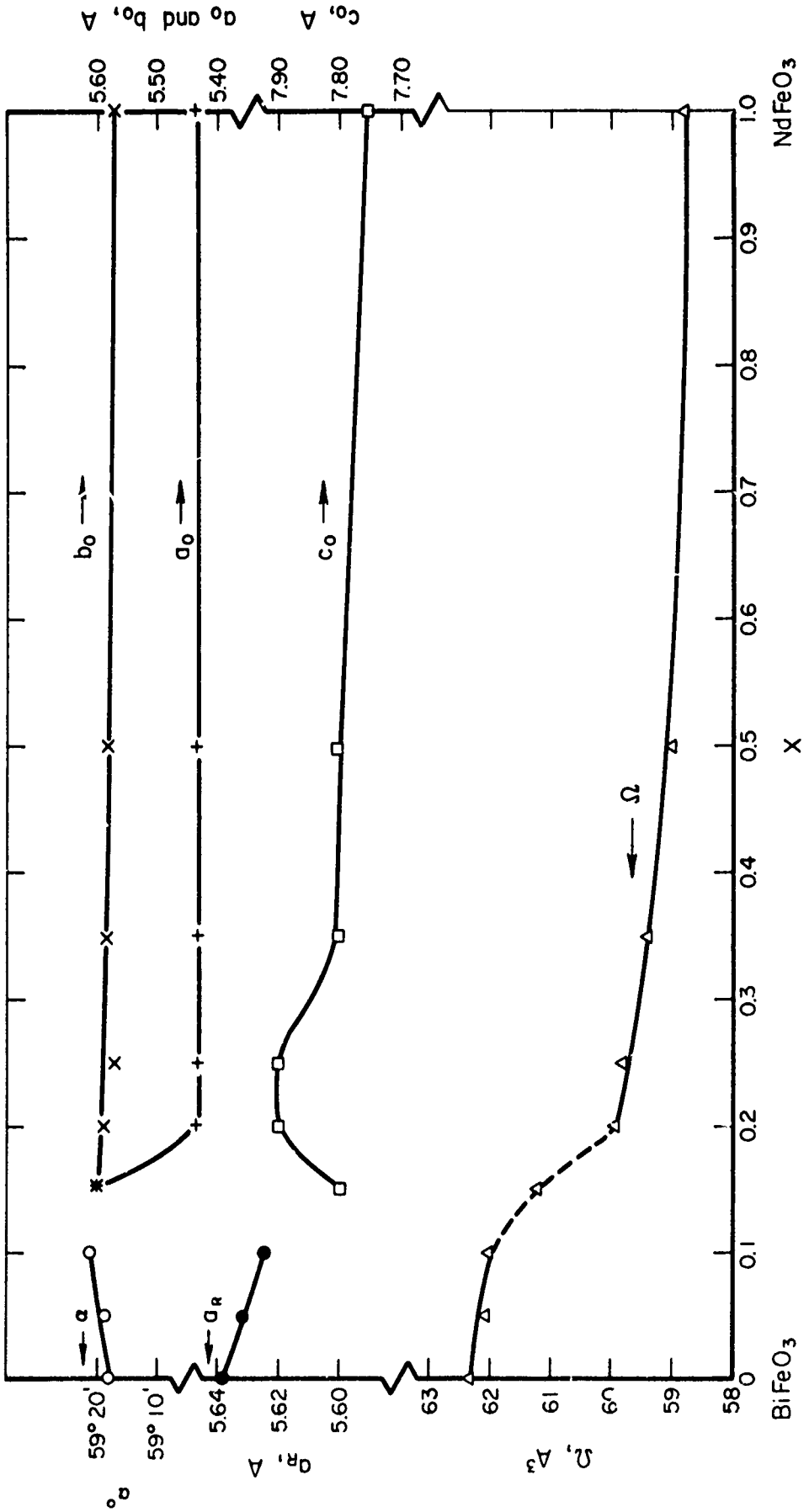

FIGURE 2

Unit-cell parameters and volumes for $Bi_{1-x}Nd_xFeO_3$.

$BiFeO_3$ phase, there is only a slight decrease in a_R and volume Ω with addition of neodymium up to x = 0.1. There is a marked decrease in volume for x = 0.15 with formation of a tetragonal phase. With further addition of neodymium, x = 0.2, the volume decreases again with formation of the orthorhombic structure of the $NdFeO_3$ type. The tetragonal structure for $Bi_{.85}Nd_{.15}FeO_3$ might actually be orthorhombic of orthoferrite type with $a_o = b_o$, but the abrupt increase in c_o and splitting of a_o and b_o values for x = 0.20 suggest that it is a narrow phase field between the rhombohedral $BiFeO_3$ and orthorhombic $NdFeO_3$ solid solutions. For $x \geq 0.2$, there is a solid solution of Bi for Nd in the $NdFeO_3$ phase. This pseudobinary system is similar to that reported by Viskov[5] for $BiFeO_3$-$PrFeO_3$. The limits of the rhombohedral and tetragonal phase fields in $Bi_{1-x}Nd_xFeO_3$ are at lower values of $x \approx 0.1$ and $x \approx 0.2$ respectively, than in $Bi_{1-x}Pr_xFeO_3$, with $x \approx 0.2$ and 0.3. In the $Bi_{1-x}La_xFeO_3$ system,[4] the rhombohedral solid solution extended to $x \approx 0.18$ and a tetragonal phase existed from $x \approx 0.18$ to 0.54. This shift in the limits of solid solutions can be accounted for by the decrease in ionic radii from 1.18Å for La^{3+} to 1.14Å for Pr^{3+} and 1.12Å for Nd^{3+} and the corresponding shift from 12-fold coordination toward eight-fold coordination with oxygen in the orthoferrites.[11] Thus the solid solution of Bi^{3+} with radius 1.11Å is greatest in $NdFeO_3$ because of the closer ionic size. However, the volume decrease from $BiFeO_3$ to the $NdFeO_3$ results from the change in the coordination of the rare-earth (or Bi) ion with oxygen—12-fold coordination in $BiFeO_3$ going to 8 nearby oxygens at 2.4 to 2.6Å and 4 further-removed oxygens at 3.2 to 3.3Å in $NdFeO_3$. The small decrease in volume in solid solutions of $BiFeO_3$ cannot be explained on the basis of rare-earth ion size, which would suggest rather a volume increase. However, some shifts in the cation displacement and the oxygen positions with solid solution of a rare earth presumably account

for the volume decrease. Such shifts in cation and oxygen positions probably are in the direction of reducing the disparity in Bi-O and Fe-O distances in $BiFeO_3$ as noted above and thus reduce polarization, ferroelectric Curie temperature, and electric coercivity.

New Phase As discussed above, a new ternary phase was found in the Bi_2O_3-Fe_2O_3-Nd_2O_3 system. This phase, as indicated in Fig. 1, occurs for nominal compositions of $Bi_{1-x}Nd_xFeO_3$, $0.15 < x < 0.5$, which are deficient in bismuth by about 6 percent. Thus, according to analysis for $x = 0.25$, the composition is $Bi_{.66}Nd_{.25}FeO_{3-\delta}$ where the exact oxygen content was not determined. The X-ray diffraction data of this phase can be indexed for a tetragonal structure with $a_o = 3.90$Å and $c_o = 9.02$Å. This gives about a 10 percent volume increase over the orthoferrite solid solution $Bi_{.75}Nd_{.25}FeO_3$. The crystal structure has not been worked out without single crystal data. However, it does not appear to be related to the cubic perovskite structure with just bismuth defects.

Magnetic Properties

All the samples of (Bi, Nd) ferrites on which magnetic susceptibility measurements were made showed strong thermomagnetic effects similar to those first reported in $NdFeO_3$ by Watanabe[12] and found in other mixed rare-earth-bismuth ferrites by other workers.[4,5] Since the magnetic properties that will be measured thus depend on the thermal and magnetic history of the sample (most importantly on whether it has cooled through the ordering temperature in a magnetic field), it is necessary to specify a measuring procedure which will enable one to compare samples of different compositions. The procedure we have adopted is that of gradually increasing the temperature and at each temperature of measurement cycling the magnetic field until a linear variation of total

magnetization with field is obtained. Thus at each temperature, one measures the saturation magnetization that can be obtained for various fields at that temperature, and these data can be analyzed in the usual way to give the apparent remanent magnetization and the high-field susceptibility. Once the ordering temperature has been surpassed and the maximum measurement temperature reached, the sample is cooled either in the residual field of the magnet (a few oersteds) on a strong field (10 kOe) and the susceptibility again measured at room temperature. In several cases, susceptibility measurements were made during the cooling part of the cycle also. The only significant change from the heating cycle was the expected increase in the moment at all temperatures below the Curie point. It was found that cooling in the residual field led to an increase in the room-temperature magnetization by a factor of around 1.2 to 2, while cooling in a high field could increase it by a factor of 3 or so. Since the magnetic transition temperatures for these materials are in the range 350 to 400 C, the measurements have been made from room temperature to around 500 C. Much above 500 C, there is some danger of dissociation of the compounds.

Some of the results of these experiments are shown in Figs. 3-5. In Figs. 3 and 4, the reciprocal of the high-field susceptibility of several compositions is shown. Two graphs have been used for clarity, since all the magnetic transitions take place in the same narrow temperature range between about 360 and 410 C. These transitions, substantially antiferromagnetic but with weak associated ferromagnetism in most cases, would appear to be of first order for $x \leq .2$. Differential thermal analysis on samples with $x = 0$ and $x = .15$ did not, however, reveal any evidence of latent heat. The largest jump in susceptibility at the ordering temperature occurs for the orthorhombic sample $x = .2$. It is possible that the orthorhombic-tetragonal phase boundary is not vertical and

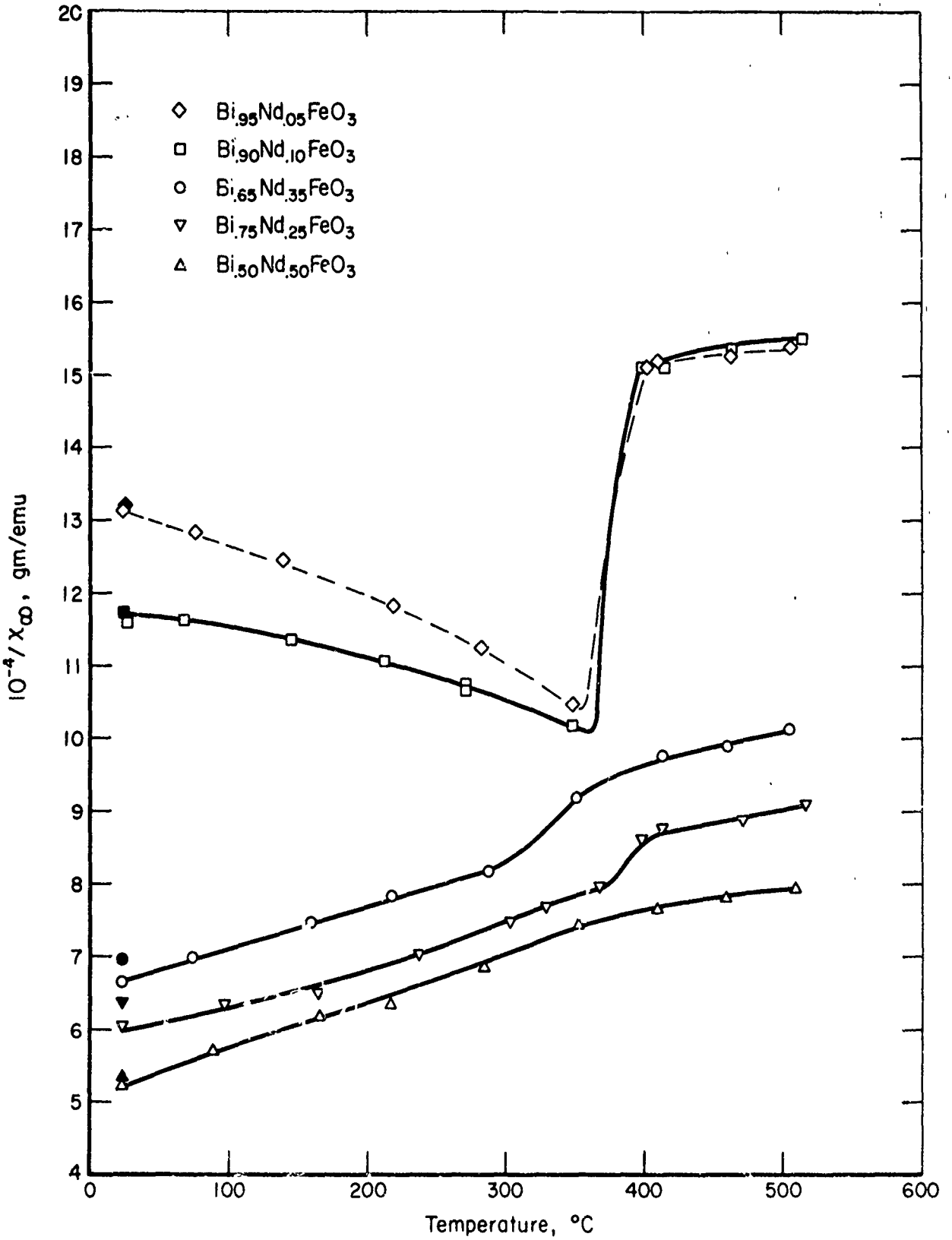

FIGURE 3

Inverse high-field susceptibilities for $Bi_{1-x}Nd_xFeO_3$. Solid data points are values to which inverse susceptibilities return after one cycle with cooling in field as described in text.

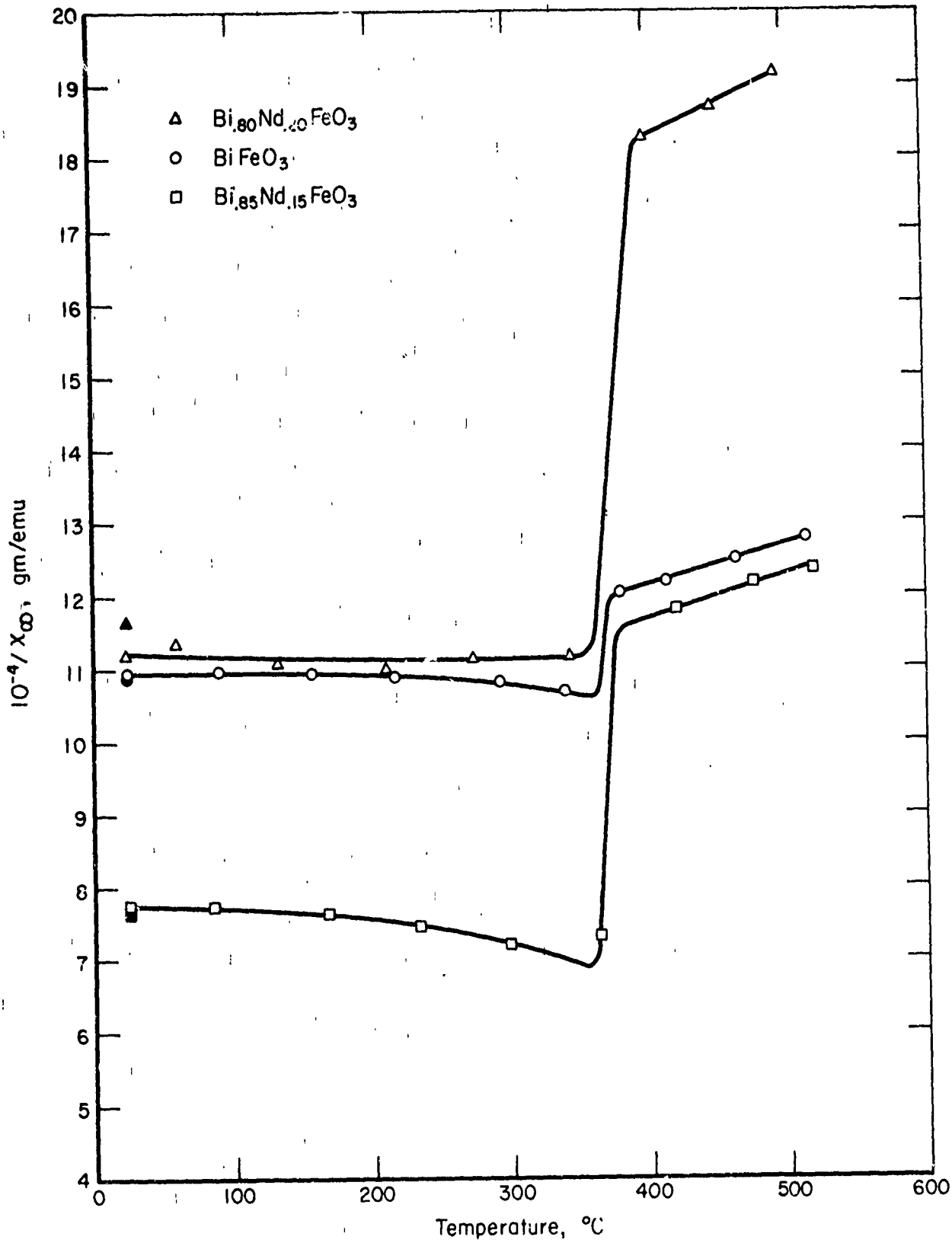

FIGURE 4

Inverse high-field susceptibilities for additional compositions in the $Bi_{1-x}Nd_xFeO_3$ system.

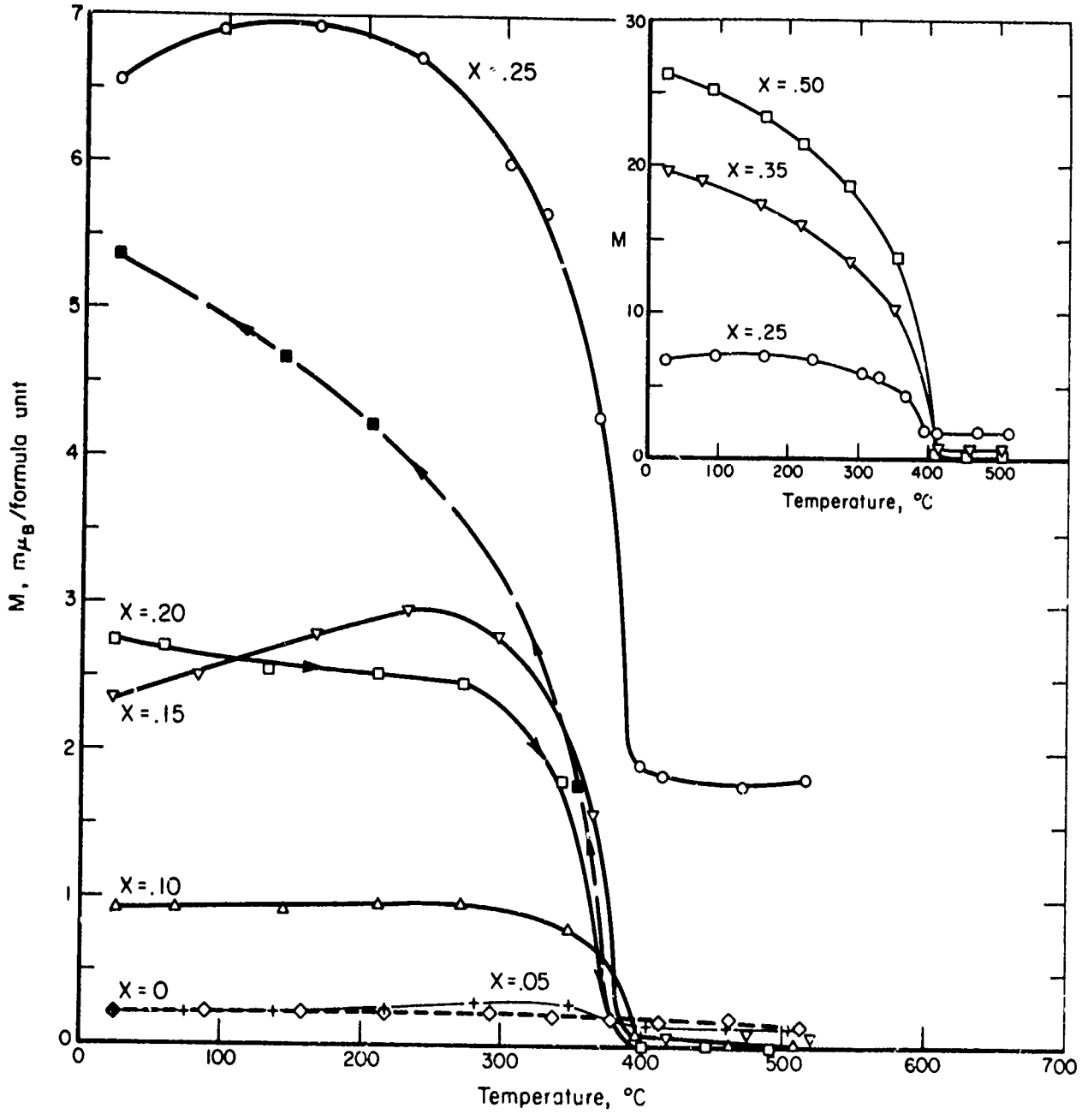

FIGURE 5

Remanent magnetization of $Bi_{1-x}Nd_xFeO_3$ as function of increasing temperature from room temperature to 500 C. For x = .2, the increased magnetization found on cooling in the residual field of the magnet is also shown.

that the sample switches over to the tetragonal phase at or near the magnetic phase transition. The room-temperature susceptibility appears to vary in a rather irregular way with composition, but little significance should be attached to this for the following reason: the samples were prepared with excess Bi_2O_3 which was subsequently leached out with nitric acid. Bi_2O_3 is strongly diamagnetic and the presence of small amounts (say up to 2%) of this material in some of the samples could rearrange the curves so that $\chi_\infty^{-1}(RT)$ decreased smoothly with increasing x. The presence of small amounts of $Bi_2Fe_4O_9$ in a few of the samples should not have greatly affected the susceptibility measurements. This material orders antiferromagnetically a little below room temperature.

In Fig. 5, the apparent spontaneous magnetic moments are shown for the same samples as in Figs. 3 and 4. The strong diminution in the magnitude of the moment at the magnetic ordering temperature in all cases except x = 0 indicates that it is weak ferromagnetism of the (Bi,Nd) ferrite that is being observed, and not the effect of some impurity. The relatively large moment of the x = .25 sample above the transition temperature is believed to result from the presence of a small amount of Bi-doped Nd iron garnet. There are several reasons for believing that the small apparent moment in $BiFeO_3$ is not intrinsic, but is rather the result of an impurity, probably γ-Fe_2O_3:

1) There is no noticeable diminution in the moment at the Néel temperature (365 C).
2) The magnitude of the moment varies slightly from sample to sample.
3) After cooling through the Néel point in a field of 10 kOe, the apparent room-temperature moment was increased only about 30%, not a significant amount in view of the moment's smallness to begin with.

We are convinced that there is no moment as large as 10^{-4} Bohr magnetons per Fe^{3+}-ion in pure $BiFeO_3$. This is in disagreement with the results of Tomashpolskii et al.,[14] who claimed to find a small moment in $BiFeO_3$ samples prepared, as were ours, in oxygen atmosphere. This claim was later withdrawn,[15] but that was done on the basis of an erroneous assumption concerning the $BiFeO_3$ crystal structure.

The most interesting result of these measurements is the occurrence of small moments in samples having the rhombohedral, and presumably ferroelectric, $BiFeO_3$ structure. This moment, about 1 $m\mu_B$ per magnetic ion in $Bi_{.9}Nd_{.1}FeO_3$, could be increased to about 3 $m\mu_B$ in that material by thermomagnetic annealing. It is possible this could be increased further by replacement of some of the ions by aluminum[16] or perhaps gallium or chromium. The presence of any moment in $Bi_{.95}Nd_{.05}FeO_3$ is somewhat more doubtful, but there does seem to be a definite drop in the magnetization near 400 C which leads us to think there may be a moment of around .1 $m\mu_B$ in this material. The moment in the $Bi_{.9}Nd_{.1}FeO_3$ sample, at least, seems to be much too large to be due to unsuspected tetragonal- or orthorhombic- phase impurities. We can only speculate about the origin of the moment. The overall structural changes on introducing small amounts of neodymium, as shown in Fig. 2, are very small. It is possible that variations in local environment occuring when some Bi ions are replaced by Nd are sufficient to allow a moment to form. Such local environment effects were suggested as a possible cause of weak ferromagnetism by Néel many years ago, but they have not to our knowledge been conclusively shown to be responsible in any particular case. The regularization of the Fe-O distances, discussed previously, which appears to occur when Nd is introduced, certainly affects the iron-iron superchange and thus may lead to the observed weak ferromagnetism. This probably can be considered in part as a local environment effect.

Another point of some interest is the continuing increase in apparent moment with increasing Nd concentration. This is strongly at variance with the results of Viskov et al.[5] on $Bi_{1-x}Pr_xFeO_3$, where the moment reaches a maximum for x = .25 and then decreases rapidly at least to x = .6. In $Bi_{1-x}La_xFeO_3$, there appears to be a more monatomic increase in moment with rare-earth concentration,[4] and there may also occur a small moment in the rhombohedral phase, not observed in the praseodymium-containing samples.

Susceptibility measurements were made on several other samples not previously discussed. A sample of $BiFeO_3$ grown from flux in a thick-walled Ni crucible (# 29528-10 of Table I) showed a moment that could be attributed to the presence of about 0.3% of a nickel-iron spinel, $NiFe_2O_4$; impurity.[17] This amount of spinel would account for about 0.07% nickel in the sample, while optical emission spectroscopy showed about 0.1 ± .05%. Thus there seems to be little tendency for the nickel to enter the rhombohedral $BiFeO_3$ phase. The susceptibility of one new-phase sample (#28886-85B) was also measured. This sample had a small moment which was attributed to garnet-phase impurity. The high-field susceptibility showed a break in slope at around 370 C, rather than the discontinuity typical of the other samples.

We did not attempt to determine the trend in the magnetic ordering temperature or the high-temperature paramagnetic moment as the Nd content of the samples was varied, as there were insufficient data points to do this accurately.

Rare-Earth Manganites and Chromites

At the close of last year, our study of the rare-earth manganites and chromites, and of their solid solutions with each other and with the orthoferrites, was nearly completed. Two principal questions remained:

1) Is there any magnetic moment produced in hexagonal, ferroelectric rare-earth manganites when a small number of the manganese ions are replaced by chromium?
2) Can it be definitely ascertained whether the rare-earth orthochromites are ferroelectric at room temperature, or can it even be established that these materials possess the requisite acentricity?

The first of these questions has been answered in the negative, at least for Yb chromite-manganites, by a comparison of measurements on different hexagonal-phase samples, of approximate composition $YbMn_{.95}Cr_{.05}O_3$, which showed variations in apparent magnetization too large to be attributable to anything but effects of an impurity, probably Mn_3O_4 with a little dissolved chromium.

The second question still has not been answered. To determine whether acentricity was present, we were led to prepare single crystals of ytterbium orthochromite and to make second-harmonic-generation measurements on these samples and on sized powders derived from them. This work is described in the following paragraphs.

Growth and Characterization of $YbCrO_3$ Crystals

The objective of the work on the growth of single crystals is to obtain single crystals of sufficient size for tests of acentricity and ferroelectricity. Previously, it had been decided that fluxes containing Pb or Bi would be avoided, if possible, since traces of these elements could greatly complicate interpretation of tests by affecting electrical properties of the material and since Pb-based fluxes have been found unsatisfactory for the manganites.[18]

Accordingly, in our earlier work, we tried various B_2O_3-based fluxes, Na_2WO_4-based fluxes, and finally Bi_2O_3 flux for growth of $YbCrO_3$, $YbMnO_3$, and $YbCr_xMn_{1-x}O_3$ mixed crystals; this exploratory work failed to yield sizable crystals.

In view of these results, we decided to proceed with Pb-based flux growth to obtain $YbCrO_3$ crystals. Thus far, one crystal-growth run has been made. In this experiment, the Wanklyn method[19] was used. The starting mixture in this method consists, on a mole-fraction basis, of 1 Yb_2O_3, 1 Cr_2O_3, 10 Pb, .1 PbO_2, and 1 B_2O_3. This mixture was placed in a Pt-Rh crucible in an oxygen atmosphere and was melted and homogenized at 1250 C, then held at this temperature for 10 days to evaporate the solvent slowly. The $YbCrO_3$ crystals grown from Pb-based flux were approximately cubic in shape with sizes about 1.5 to 3 mm on edge. In a section of an aggregate, there were some inclusions of lead oxide. A cross-section of an apparent single crystal, on the other hand, showed a string of apparent small round inclusions which were shown by electron-microprobe analysis to be empty pores. No lead was detected within the single crystal. However, inclusions of Yb_2O_3 were found.

Second Harmonic Generation

As mentioned above, and discussed in previous reports, determination of acentricity is helpful in attempting to establish the presence of ferroelectricity. The observation of any effect absent in centrosymmetric materials is generally sufficient, together with X-ray data, to place a material in a pyroelectric crystal class; and the effect under study will usually show some anomalous behavior in the region of the ferroelectric ordering temperature. Several methods including temperature dependence of the dielectric constant and the electrical resistivity, piezoelectric resonance experiments and pyroelectricity

tests have been employed more or less unsuccessfully for determining acentricity in the rare-earth chromites and manganites prepared in this program. In most cases free-carrier screening of the lattice response to electric fields or mechanical stresses has precluded observation of the desired effect. The most direct method for overcoming the problem of free-carrier screening in these low-activation-energy semiconductors is to perform tests at frequencies very much higher than the free-carrier relaxation frequency so that these carriers cannot react fast enough to negate the lattice response. This condition is easily satisfied at optical frequencies for all but metallic materials, and the generation of second-harmonic signals using intense laser sources in a definitive test for the existence of acentricity in non-cubic materials. The only limitation of this technique is that the specimen may be so highly absorbing at the harmonic wave-length that SHG signals cannot be detected.

We have constructed apparatus, similar to that described by Kurtz and Perry,[20] for detecting the measuring SHG in powder specimens as well as in crystals. To date we have employed the 1.06μ emission of a Nd-glass laser and the 0.6945μ emission of a high power ruby laser for generation of SHG at 0.53μ and 0.3477μ respectively. We have detected SHG in a variety of test materials having a wide range of SHG efficiencies. These include KIO_3, $NaNO_3$ and $Gd_2(MoO_4)_3$ which have SHG efficiencies of about 2000, 100, and 20 relative to a quartz standard. We have also observed SHG in quartz powder, but quantitative measurements are difficult because, in order to detect these much weaker signals, it is necessary to use high input intensities, and the point where the SHG signal becomes obscured by multiple fluorescence is rapidly reached. This means that for fixed detector sensitivity the effective range of input intensity over which one can observe a square-law dependence of the SHG intensity on the input intensity decreases with decreasing SHG efficiency; for KIO_3, SHG signals could be

observed as the input intensity was changed by three orders of magnitude or more, while for quartz the effective input-intensity range was limited to about one order of magnitude. This problem can also exist for materials having high "intrinsic" SHG efficiencies if there is appreciable absorption at the fundamental and/or harmonic frequencies. We have emphasized these points for two reasons. First, the rare-earth chromites and manganites are low-activation-energy semiconductors which at room temperature are fairly absorbing in the range .3 to 1.0 microns. Second, in order to determine acentricity in an unknown material by establishing a square-law dependence of the SHG intensity on input intensity, it is generally necessary to vary the input intensity by at least two orders of magnitude because random spatial variations in the intensity of the laser pulses produce large scatter in the SHG signals. These problems have hindered our efforts to establish the existence of acentricity in $YbCrO_3$.

Using the ruby laser primarily, we performed SHG experiments on single-crystal, polycrystalline and powder specimens of $YbCrO_3$. Single crystals and polycrystalline chunks were obtained from the flux-grown material while powder specimens were prepared from both the flux-grown material and the sintered material. In all cases, problems of sensitivity and multiple fluorescence restricted the range of input intensity to about a factor of ten change. Although the SHG signals clearly display a stronger-than-linear dependence on input intensity, a square-law dependence is difficult to establish unambiguously because of the large amount of scatter in the data. It is possible that a careful statistical analysis of the data may convincingly demonstrate the presence, or absence, of second-harmonic output. For example, in one experiment on sintered powder, the best straight-line fit to a log-log plot of the output signal as a function of the input monitor-signal had a slope of 2.5 ± .25 (standard deviation), and

the correlation of the output o- -he input for this line was + .92 ± .03. Of course, the correlation coefficient would be lower for a line forced to have a slope of 2; still, these results seemed to us sufficiently encouraging to warrant taking additional data, the analysis of which is still in progress.

NARROW-BAND NARROW-GAP MATERIALS

Background

A number of possible applications for solid-state integrated circuits have not yet been realized because high-speed switching elements have not been developed. Consequently, a great deal of interest has evolved in materials which undergo abrupt semiconductor (or insulator)-to-metal transitions. Of greatest practical importance are materials in which such transitions can be induced by an applied electric field. In addition, it is highly desirable that the switching mechanism be purely electronic without the necessity for secondary (usually slower) mechanisms such as thermal effects which play an important role in the chalcogenide glasses. To date, electric-field-induced electronic transitions appear to have been observed only in V_2O_3 and VO_2. In the latter case, it is said that the transition results from huge piezoelectric strain,[21] but this seems to contradict the observed crystal symmetry.[22] One might expect purely electronic transitions in materials which possess loosely-bound localized excited states, and indeed such states have been invoked to explain the electrical behavior of certain compounds containing divalent samarium ions. In particular, the gradual semiconductor-to-metal transition as a function of temperature in SmB_6 has been interpreted in this way.[23] Maple and Wohlleben[24] have pointed out that the metallic state of SmB_6 may be characterized by rapid fluctuations, the fluctuation time being of order $\hbar$ divided by the energy splitting between the localized Sm^{2+} ground state and the more loosely-bound Sm^{3+} excited state. Using the temperature dependence of the electrical resistivity to obtain an estimate of the energy splitting, these authors predict a fluctuation time of order 10^{-12} seconds, and argue that such behavior can explain the seemingly conflicting results

of Mossbauer,[25] magnetic susceptibility[26] and soft X-ray[27] experiments on SmB_6.* Nickerson et al.[23] suggested that a semiconductor-to-metal transition involving localized states of the samarium ion might be unique to the SmB_6 lattice owing to the extreme rigidity of the boron sublattice. However, rather similar, although pressure-induced, transitions** have been observed in SmS,[28] SmSe,[28] and SmTe,[29] and these authors have argued that these transitions involve the same two electronic states of the samarium ion. Unfortunately, the metallic states of these samarium monochalcogenides have not been investigated to the same extent as the metallic state of SmB_6 because experiments must be performed at high pressure. Furthermore, recent magnetic susceptibility[30] and electron spin resonance[31] experiments have created some controversy (discussed below) about the degree of localization of the 4f electronic states of the samarium ions in these materials. In order to help resolve this controversy, we initiated a systematic study of the Se^{77} nuclear magnetic resonance in SmSe and in SmS_xSe_{1-x} pseudo-binary alloys. During the period covered by this report most of our research effort on narrow band-narrow gap compounds was devoted to this NMR study while smaller efforts were concerned with the problem of cathodoluminescence and preliminary measurements of the Hall effect and thermoelectric power of these materials. The following section describes recent work on growth of single crystals of Sm chalcogenides while the succeeding section contains a discussion of our NMR results. Finally, a short discussion is given of our cathodoluminescence measurements.

---

* Since a fluctuation time of order 10^{-12} sec is much shorter than the Larmor period, this model also explains our failure to observe the electron spin resonance of Sm^{3+} in SmB_6 as discussed in a previous report.

** At ambient pressure and temperature SmSe and SmTe are semiconductors having resistivities on the order of 10^3-10^4 ohm cm. Upon application of pressure to 50 kbar both materials undergo a gradual transition to a metallic state in which the resistivity is of the order 10^{-4} ohm cm. On the other hand, SmS exhibits an abrupt transition at 6.5 kbar, but because the activation energy of the semiconducting state is extremely low, the resistivity change is only about a factor of three or four.

Sm Chalcogenide Crystal Preparation

Prior to this program, samarium monochalcogenides had been prepared at Battelle[32] by reacting samarium metal filings or turnings with the Group VI elements at moderate temperatures (400 - 850 C) in sealed silica ampoules, then melting the materials in tantalum crucibles in an inert atmosphere to form polycrystalline ingots. Such ingots usually contained large crystals and yielded single-crystal specimens of acceptable size. In the early work on the present project, this method was applied to the preparation of SmS, SmSe, and SmS_xSe_{1-x} mixed crystals. However, it was found that materials melted in an unsealed tantalum crucible in an inert atmosphere tended to lose samarium preferentially and to contain chalcogen-rich second phases. It was observed metallographically that this second phase was intergranular. Electron-microprobe analysis showed it to be samarium oxysulfide, Sm_2O_2S. The metallographic examination also revealed some spherical metallic inclusions, which were found to be tantalum, or a tantalum-rich alloy.

Several modifications of the apparatus were necessary to yield stoichiometric, inclusion-free crystals. To prevent loss of samarium, the final melting and crystal growth steps were carried out in Ta crucibles which had been evacuated and then sealed by electron-beam welding. To eliminate the tantalum inclusions, and also to improve the reliability of the electron-beam welds, a tantalum baffle was placed in the crucible between the sample and the weld-seal region, and new accessories were provided to improve cooling during the electron-beam welding step. To eliminate oxysulfide contamination, the sulfur was deoxidized before use, and maintained in a strictly oxygen-free environment. These measures appeared to be successful, and single-phase specimens, typically consisting of a few good-sized single crystals, of SmS, SmSe, $SmS_{.75}Se_{.25}$, $SmS_{.6}Se_{.4}$,

and $SmS_{.4}Se_{.6}$ were prepared according to the following procedure:

High-purity selenium and sulfur (nominal purities 99.999%) and nominally 99.9% pure samarium were employed. The sulfur was first deoxidized by multiple vacuum melting in a Teflon boat coated with pyrolytic carbon to remove oxygen as the volatile sulfur oxides. All subsequent handling steps were conducted in an inert atmosphere.

The proper proportions of the elements were reacted in an evacuated, sealed silica ampoule at 400 C, then 500 C, then 600 C with the temperature being increased stepwise over a 75-hour period.

In a glove box, the material was transferred to a tantalum crucible provided with a baffle and a close-fitting top. The crucible and contents were sealed in a suitable container under the inert-gas glove-box atmosphere for transport to the electron-beam welder where the crucible was weld-sealed after an overnight pumpdown.

The tantalum crucible then was suspended in a sealed silica ampoule in a pure helium atmosphere. By use of rf heating, the material was melted, with maximum temperature 2050 C to 2150 C, depending on the composition. The maximum temperature was held for an homogenization period of about 15 minutes; then, with the sample region in a temperature gradient of about 40 C per cm, the power was turned down in such a way as to give a cooling rate of 70-90 C per hour through the liquid-solid transition range. Samples prepared this way were used in the magnetic resonance studies to be described next.

Se^{77} NMR in SmSe and Sm_xSe_{1-x} Alloys

We have used nuclear magnetic resonance to measure the temperature dependence of the local internal magnetic field at the selenium site in SmSe over the temperature range 77 to 470 K. The results are displayed in Figure 6 as a

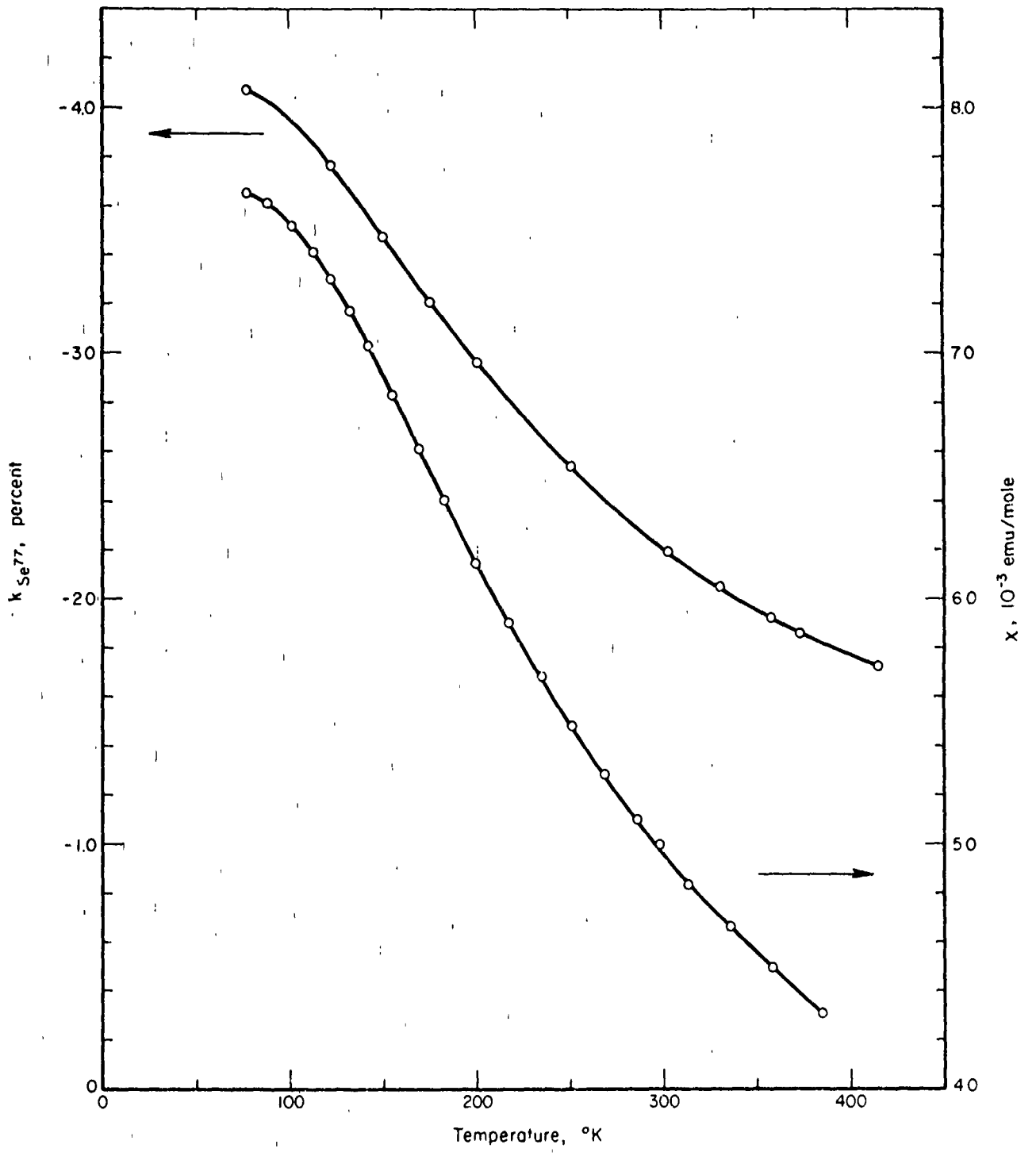

FIGURE 6

Se^{77} magnetic resonance shift, k, and magnetic susceptibility, χ, in SmSe.

percentage shift of the effective internal field relative to the corresponding field at a Se^{77} nucleus in a diamagnetic medium. For comparison the temperature dependence of the magnetic susceptibility of the same SmSe material is also shown in Figure 6. The striking similarity between these two curves, coupled with the fact that the shift values are negative and very large, leads one to hypothesize that the internal field at the selenium site is dominated by localized spins on the samarium sites. This means that NMR experiments should provide valuable information about the localized nature of the electronic states of the samarium ions and possibly also about the conduction mechanisms in these materials. The conventional method for testing the above hypothesis is to plot the resonance shift as a function of the susceptibility using temperature as an implicit parameter. However, because the multiplet structure of the Sm^{2+} ion ($4f^6$ configuration) has a non-magnetic ground state (J = 0) and a nearby first excited state (J = 1), the magnetic susceptibility is not proportional to the expectation value of the samarium spin. Thus, the local magnetic field at the selenium site due to indirect exchange interactions between the samarium spins and the selenium nuclei is not expected to be proportional to the susceptibility over a large temperature range. This unusual feature provides an advantage in determining information about the spin-orbit energy (the energy difference between the J = 0 and J = 1 states) and the Sm-Sm exchange energy in the samarium monochalcogenides because the NMR and magnetic susceptibility measurements yield separate data from which these important parameters may be extracted.

To make these remarks more quantitative and to demonstrate the necessity for incorporating exchange in the analysis of our NMR data, we consider the magnetic properties of the Sm^{2+} ion. Van Vleck[33] has shown that the susceptibility of a $4f^6$ ion is given by:

$$\chi_{VV} = \frac{N\beta^2}{2E_1} \frac{W}{Z} \qquad (1)$$

where $W = 16 + (9x - 1)\, e^{-x} + (45x - 5/3)\, e^{-3x}$

$+ (126x - 7/3)\, e^{-6x} + (270x - 9/3)\, e^{-10x}$

$+ (495x - 11/3)\, e^{-15x} + (819x - 13/3)\, e^{-21x}$

$Z = 1 + 3e^{-x} + 5e^{-3x} + 7e^{-6x}$

$+ 9e^{-10x} + 11e^{-15x} + 13e^{-21x}$

$x = E_1/kT$, and

E_1 = spin-orbit energy, i.e. the energy difference between the J = 0 and J = 1 states of the multiplet .

In the absence of Sm-Sm exchange interactions, the susceptibility of SmSe would be expected to obey the following relation*

$$\chi = \chi_o + \chi_{VV} \quad , \tag{2}$$

where χ_o contains the diamagnetism of the ion cores and small contributions from the free carriers.

Bucher et al.[30] reported that by neglecting free carriers and assuming a diamagnetic contribution of $-.07 \times 10^{-3}$ emu/mole, Eq 1 and 2 with a spin-orbit energy E_1 of about 380 K fit their measured susceptibility to within one percent over the entire range from 0 to 400 K. However, such a value for the spin-orbit energy is disturbing because the value for a Sm^{2+} free ion is 421 K,[34] while the measured value for Sm^{2+} in various alkali-halide hosts is about 415 K.[35] Furthermore, the neglect of exchange has been challenged by Mehran et al.[31] who observed large g shifts in the electron spin resonance of Eu^{2+}, Gd^{2+} and Mn^{2+} in SmSe. These facts stimulated Birgeneau et al.[36] to reanalyze the susceptibility data of Bucher et al.[30]. Using the molecular-field approximation, they calculated

---

* The small effect of the cubic crystal field on states for which J > 2 has been neglected.

the exchange-modified susceptibility at zero degrees kelvin only, and compared this result with an estimated experimental value obtained by extrapolating the observed susceptibility to absolute zero. Adopting a spin-orbit energy of 415 K ± 6 K, they obtained a value* of + 2.1 ± 0.5 K for the Sm-Sm exchange energy in SmSe. But these authors did not consider the degree to which this new model correlated with the observed susceptibility at finite temperatures. To check this point, we modified eqs. 1 and 2, following the procedures outlined by Wolf and Van Vleck,[37] to incorporate the effect of exchange. The results are:

$$\chi = \chi_o + \frac{N\beta^2}{2E_1}\left[\frac{W}{Z} + \frac{\lambda}{E_1}\left(\frac{Y}{Z}\right)^2 \frac{1}{\left[1 - \frac{\lambda}{E_1}\frac{U}{Z}\right]}\right] \qquad (3)$$

where $Y = 16 + (3x - 1)\, e^{-x} + (15x - 5/3)\, e^{-3x}$

$+ (42x - 7/3)\, e^{-6x} + (90x - 9/3)\, e^{-10x}$

$+ (165x - 11/3)\, e^{-15x} + (273x - 13/3)\, e^{-21x}$,

$U = 16 + (x - 1)\, e^{-x} + (5x - 5/3)\, e^{-3x}$

$+ (14x - 7/3)\, e^{-6x} + (30x - 9/3)\, e^{-10x}$

$+ (55x - 11/3)\, e^{-15x} + (91x - 13/3)\, e^{-21x}$, and

λ = exchange energy defined by the relation $\beta H_{exch} = -\lambda \langle S \rangle$.

Allowing E_1 and λ to vary independently while performing a least-squares fit of eq. 3 to all our susceptibility data yields best-fit values of $\lambda = 0.25$ K, $E_1 = 390$ K, and $\chi_o = -0.099 \times 10^{-3}$ emu/mole; for these values of the parameters

---

* The value reported by Birgeneau et al. is -4.2 ± 1.0 K, but since our definition of the exchange parameter differs from theirs by a factor of -1/2, we list here the appropriate value for comparison with later calculations in the text.

the largest single error in χ over the entire range of temperature investigated is 0.24%. Alternatively, if we assume a fixed spin-orbit energy of 415 K ± 6 K, we can find no value of λ which gives agreement to within 0.5% over the same range. Thus without considering further modifications of the model, the existence of appreciable Sm-Sm exchange does not appear to be consistent with the magnetic susceptibility at elevated temperatures. It is easy to see that inclusion of the Pauli susceptibility of the free carriers cannot alter the situation appreciably because, in spite of the fact that the carrier concentration is a strong function of temperature, the total number of carriers is relatively small even at 400 K. Assuming a free-electron model and one carrier per Sm ion we calculate a Pauli susceptibility of about 0.04×10^{-3} emu/mole. Since the actual carrier concentration is at least a factor of 10^3 smaller than assumed above, the Pauli susceptibility is completely negligible even if we consider an exchange enhancement of 10 to 100. Before considering what we believe is likely to be the most important modification, namely, a temperature dependence of the exchange parameter, we wish to discuss the extent to which the NMR data agree with the present model.

Several authors[38] have shown that the transferred hyperfine field due to exchange interactions between a localized spin and a remote nucleus is determined by the expectation value of the z-component of the spin, $\langle S_z \rangle$, and not the expectation value of the z-component of the total angular momentum, $\langle J_z \rangle$. Therefore, to a first approximation we can express the resonance shift for the Se^{77} NMR in SmSe as

$$k = k_o + \gamma \frac{\langle S_z \rangle}{H} \quad , \tag{4}$$

where k_o contains all shift mechanisms which are not related to the 4f electrons of the samarium ion. These include core diamagnetism of the Se ion and the paramagnetism associated with free carriers.

With the inclusion of exchange, the expectation value of the z-component of the Sm^{2+} spin is given by:

$$\frac{\langle S_z \rangle}{H} = -\frac{\beta}{2E_1}\,\frac{Y}{Z}\,\frac{1}{\left[1 - \frac{\lambda\beta}{E_1}\,\frac{U}{Z}\right]} \qquad (5)$$

where all symbols are as defined previously.

Eqs. 4 and 5 show that $\langle S_z \rangle$ and k both depend upon the spin-orbit energy E_1 and the exchange energy λ but that for given values of these parameters, they have a different temperature dependence than does the magnetic susceptibility.

We have fit our experimental shift data over the temperature range 77 to 370 K to Eq. 4 by least-square analysis, considering E_1 and λ as adjustable parameters. The best fit is obtained for λ = 4.25 K, E_1 = 424 K and k_o = + 0.086%. It is surprising to find that although these results are not in good agreement with those obtained by the similar analysis of our magnetic susceptibility data, they seem to agree reasonably well with the results of Birgeneau et al.[36] for T = 0.

We now return to the question of a temperature-dependent exchange parameter. We anticipate that this effect will be important because thermal expansion coefficients for compounds having the NaCl structure are typically large and because the exchange energy is determined by a delicate balance of overlapping electron orbitals. As a first approximation, we adopt a linear model in which the exchange parameter at finite temperature is given by:

$$\lambda(T) = \lambda(0) + \left(\frac{\partial\lambda}{\partial\ell_o}\bigg|_{T=0}\right) \alpha\ell_o T \qquad , \qquad (6)$$

where ℓ_o = lattice constant, and
α = thermal expansion coefficient.

Using the results reported by Birgeneau et al. for the exchange parameters in SmS, SmSe, and SmTe at T = 0, we estimate that $\partial\lambda/\partial\ell_o|_{T=0}$ for SmSe is -22 ± 5 K/Å. We have been unable to find thermal expansion data for SmSe, but with a reasonable degree of confidence we may assume a value of about $35 \pm 20 \times 10^{-6}\ K^{-1}$, which is representative for a large number of compounds having the NaCl structure. Combining these estimates we obtain:

$$\lambda(T) \simeq 2\ K - (50 \pm 50) \times 10^{-4}\ T \quad . \tag{7}$$

Clearly, for temperatures as high as 400 K the second term on the right side of Eq. 7 cannot generally be ignored. Therefore, we modified the least-square analysis of our susceptibility data to include variations in the coefficient of the temperature term from 0 to 10^{-2} in steps of 10^{-3}. As before, the best-fit values for E_1 and $\lambda(0)$ are about 390 K and 0.25 K respectively so we still cannot reconcile the finite-temperature susceptibility data with the assumption that E_1 is 415 K ± 6 K.

In view of this result, we do not expect significant changes in the least-square analysis of the shift data upon including a temperature-dependent exchange parameter of the above form, although we plan to test this point in the near future. Instead we believe that it will be necessary to consider <u>non-linear temperature effects</u> on λ. These may arise from non-linearities in the expansion coefficient or from changes in λ due to free carriers, the number of which depends exponentially on temperature. Determination of the exact temperature dependence of the carrier concentration of course requires measurement of the transport properties. Work on such measurements, i.e. electrical resistivity, Hall effect and thermoelectric power is under way.

Cathodoluminescence

As discussed briefly in the previous report, luminescence was observed in samarium sulfide-selenide samples when they were examined in the electron microprobe. The visual intensity was found to increase with electron beam current and power density, appearing white and quite bright at high power levels. A more detailed study was conducted with a grating spectrometer (Bausch & Lomb Model 33-86-02), with resolution of about 100Å/mm, attached to the electron microprobe. Light emitted from a sample was collected by the reflecting optics of the light microscope in the electron microprobe. The spectral intensity was measured between 350 and 750 mμ with a PM-4 photomultiplier and corrected for the relative response of this phototube.

These cathodoluminescence experiments were done on cleaved faces of SmS, SmSe and $SmS_{.6}Se_{.4}$. In these experiments at varying beam current and power, the power density could be further changed by varying the beam diameter from 7.5μ to 0.8μ. The specimen was moved continuously under the electron beam at 20μ/minute. The corrected spectral intensity data shown in Figs. 7, 8 and 9 were all taken with a beam voltage of 45 kV and a minimum beam diameter of 0.8μ.

There are at least two effects involved in the cathodoluminescence. First, there is a broad-band emission with a maximum around 450 mμ. The intensity of this band increases linearly with beam current for $SmS_{.6}Se_{.4}$ and SmSe as shown in Fig. 10. In contrast, the emission from SmS appears relatively constant. It was observed that in SmS the light emission was from a larger diameter than the electron-beam focus. This may possibly indicate both electron and X-ray excitation in SmS, whereas there is only electron-induced luminescence in the selenide solid solutions. While this bluish luminescence is easily observed by eye, direct comparison at a lower voltage shows that it is at least

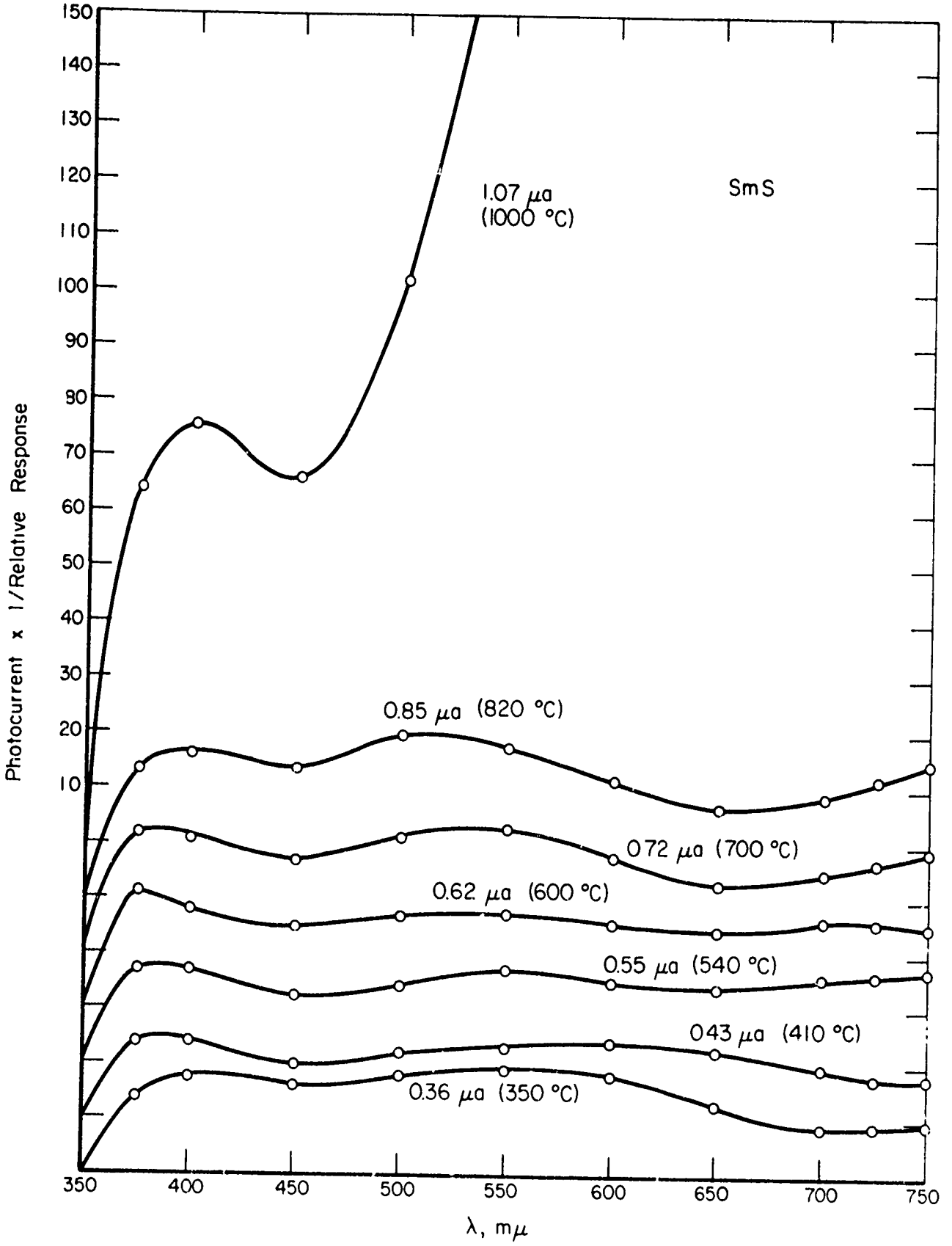

FIGURE 7

Cathodoluminescence spectra of SmS at various electron beam currents. Successive curves displaced by 10 units for clarity. Estimated temperature rise at beam focus given in parentheses. No correction for the electronic contribution to the conductivity has been made.

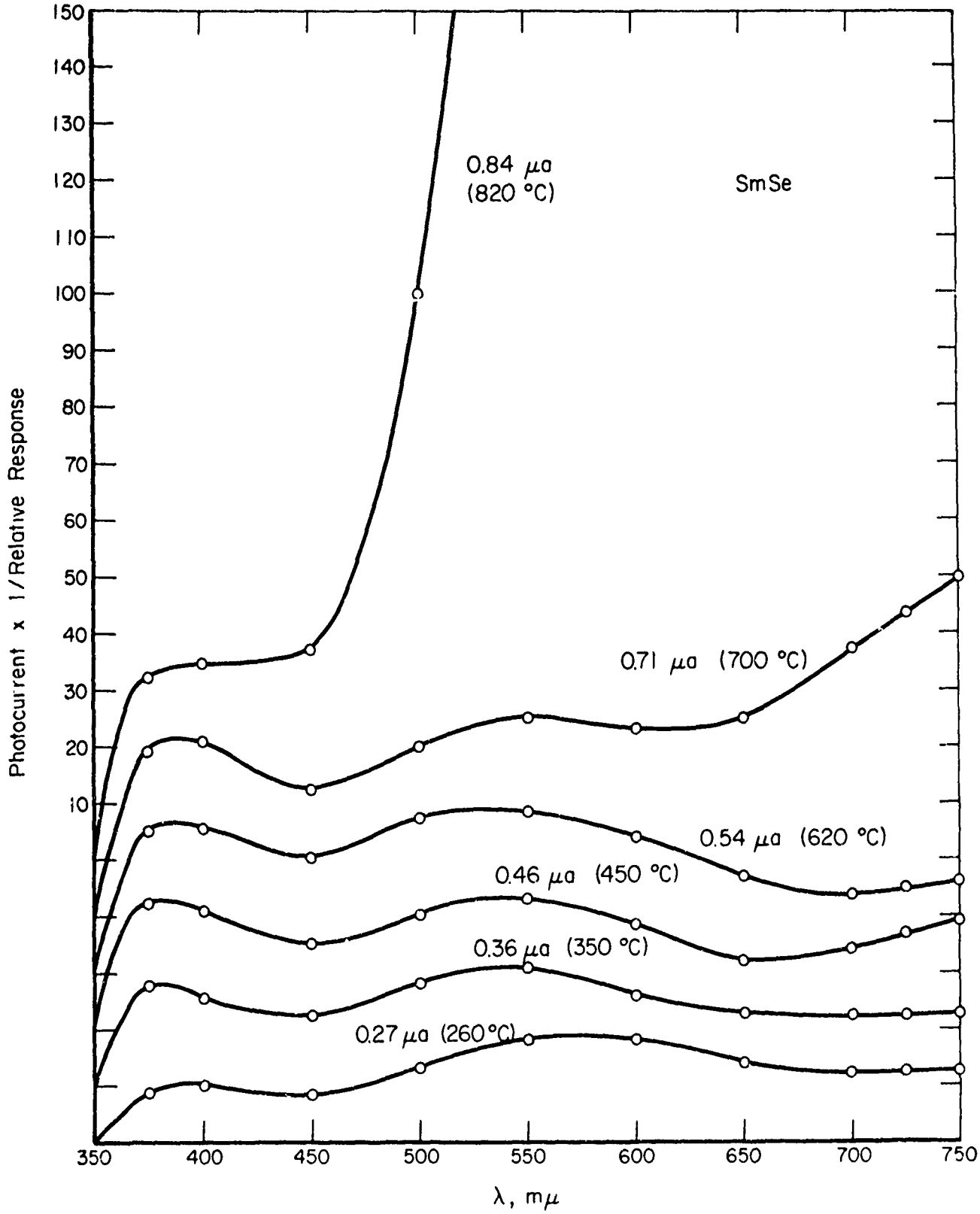

FIGURE 8

Cathodoluminescence spectra of SmSe at various electron beam currents. Successive curves displaced by 10 units for clarity. Estimated temperature rise at beam focus given in parentheses.

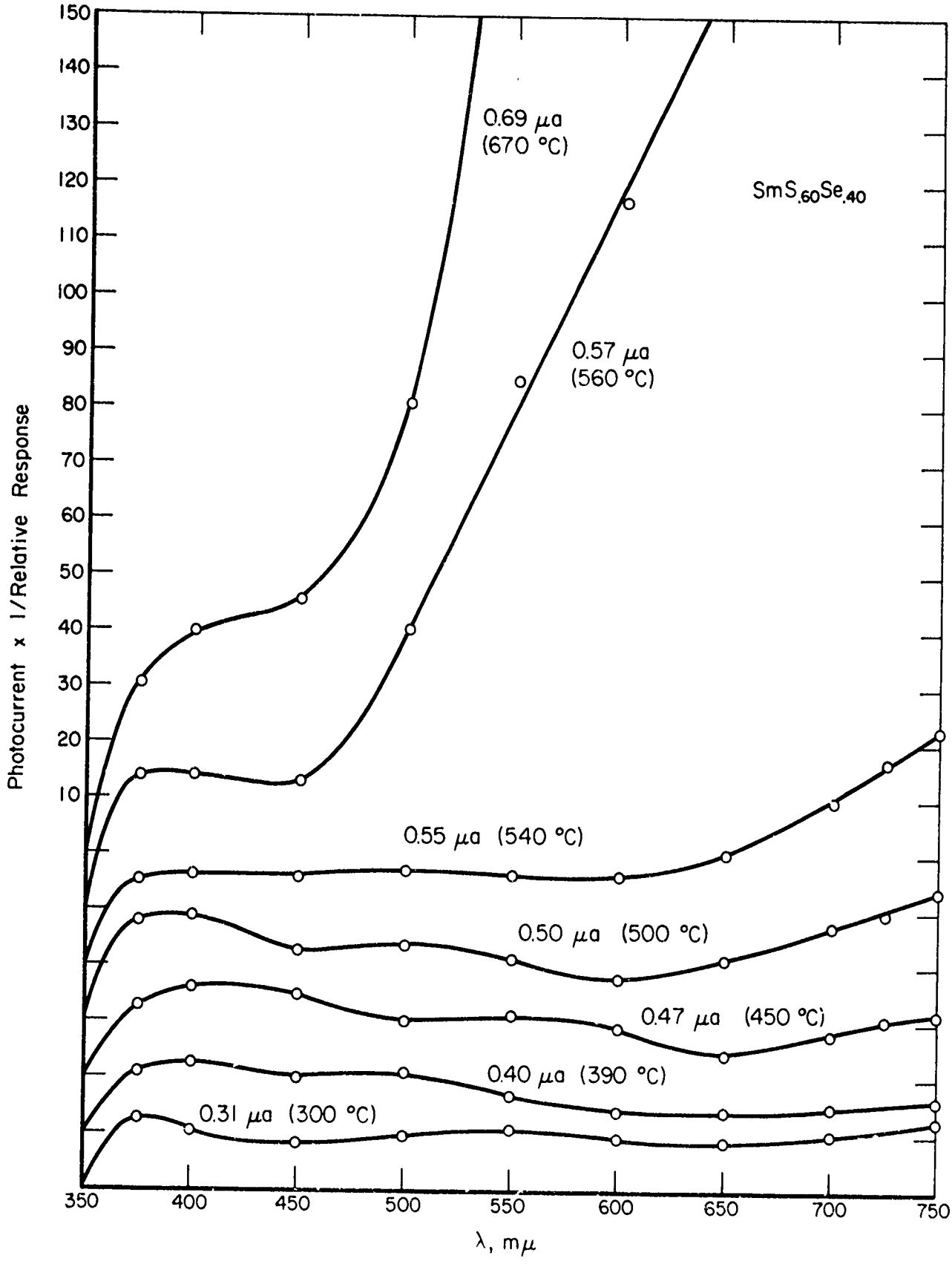

FIGURE 9

Cathodoluminescence spectra of $SmS_{.6}Se_{.4}$ at various electron beam currents. Successive curves displaced by 10 units for clarity. Estimated temperature rise at beam focus given in parentheses.

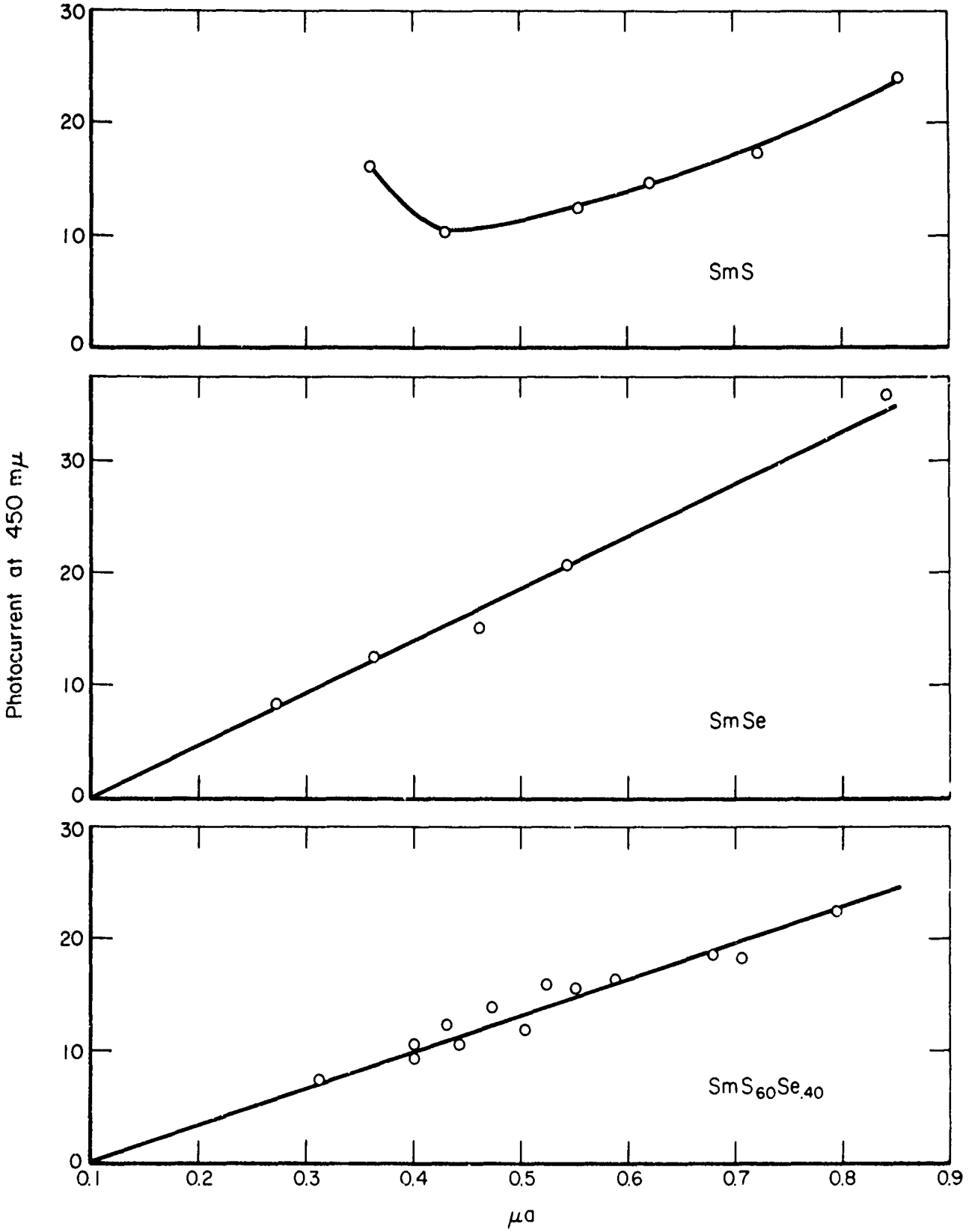

FIGURE 10

Intensity of cathodoluminescence in blue region (450 mμ) as function of electron beam current at 45 kV, 0.8μ diameter beam.

four orders of magnitude weaker than that obtained at comparable power levels in high-efficiency transparent luminescent materials, such as Gd_2O_2S. (This experiment was kindly performed by R. A. Buchanan, Lockheed Palo Alto Research Laboratory.)

At higher power densities (above 3×10^6 watts/cm^2), high-intensity luminescence, peaked in the red, appeared. This is thermally-excited emission. The maximum temperature rise at the electron-beam focus was estimated from the equation

$$T_m = 0.057\ W/C\ r_o \quad ,$$

where W is input power in watts, C is thermal conductivity in cal/cm-sec-°C, and r_o is the electron beam radius in cm. Values of T_m found this way are given in Figs. 7 to 9. This equation is based on the assumption that the electron-beam energy is converted into heat within a hemisphere whose radius is equal to that of the electron beam, i.e., 0.4 to 0.5μ. The thermal conductivity was assumed to be independent of temperature and to have the value 0.066 cal/cm-sec-°C, a value typical of many sulfides at room temperature, in all three materials. The measured thermal conductivity of SmSe is considerably lower than this,[39] and that in the mixed crystal $SmS_{.6}Se_{.4}$ should be lower still. Still, in view of the uncertainty about the radius of the energy-dissipation volume, possibly twice the incident-beam radius, to say nothing of the fact that the calculated temperature rise in these samples assuming the other conditions as before would be unreasonably high, we have not attempted any correction for this. Nor has any correction been made for the free-carrier contribution to the electrical conductivity, which should be substantial in SmS. Thus in SmS the temperature rise should be somewhat less than that calculated, while for $SmS_{.6}Se_{.4}$, it is probably greater than that calculated. This is in agreement with the observations

that there is virtually no thermal incandescence in SmS except at the highest power levels and that incandescence is found at lower power levels in the mixed-crystal sample than in either the sulfide or the selenide. The main point of the calculations, of course, is simply to show that heating these materials to incandescence with the electron beam is possible, and might reasonably be expected under these experimental conditions.

After exposure to the highest electron-beam currents the samples exhibited disturbed regions along the electron-beam trace. There was fine lateral cracking, presumably from thermal expansion stress. In $SmS_{.6}Se_{.4}$ the disturbed region had disproportionation of S and Se, leaving the center region sulfur-rich with approximate composition $SmS_{.75}Se_{.25}$. The selenium-rich regions formed narrow bands on either side of the sulfur-rich center. The samarium level was constant to within 1 percent and there appeared no significant loss of any constituent. This disproportionation may arise simply from thermal diffusion.

REFERENCES

1. G. D. Achenbach, W. J. James, and R. Gerson, J. Am. Ceram. Soc. 50, 437 (1967).

2. H. Koizumi, N. Niizeki, and T. Ikeda, Japan. J. Appl. Phys. 3, 495 (1964).

3. E. I. Speranskaya, V. M. Skorikov, E. Ya. Rode, and V. A. Terekhova, Bull. Acad. Sci. USSR, Div. Chem. Sci., 874 (1965).

4. Yu. E. Roginskaya, Yu. N. Venevtsev, S. A. Fedulov, and G. S. Zhdanov, Soviet Phys. -- Crystallography 8, 490 (1964).

5. A. S. Viskov, Yu. N. Venevtsev, V. M. Petrov, and A. F. Volkov, Inorganic Materials 4, 71 (1968).

6. J. M. Moreau, C. Michel, R. Gerson, and W. J. James, J. Phys. Chem. Solids 32, 1315 (1971).

7. S. V. Kiselev, R. P. Ozerov, and G. S. Zhdanov, Soviet Phys. - Doklady 7, 742 (1963).

8. C. Michel, J. M. Moreau, G. D. Achenbach, R. Gerson, and W. J. James, Solid State Commun. 7, 701 (1969).

9. S. C. Abrahams, S. K. Kurtz, and P. B. Jamieson, Phys. Rev. 172, 551 (1968).

10. R. L. White, J. Appl. Phys. 40, 1061 (1969).

11. M. Marezio, J. P. Remeika, and P. D. Dernier, Acta Cryst. B26, 2008 (1970).

12. H. Watanabe, J. Phys. Soc. Japan 14, 711 (1959).

13. A. G. Tutov et al., Soviet Phys. - Solid State 6, 963 (1964).

14. Yu. Ya. Tomashpolskii, Yu. N. Venevtsev, and G. S. Zhdanov, Soviet Phys. - JETP 19, 1294 (1964).

15. Yu. E. Roginskaya et al., Soviet Phys. - JETP 23, 47 (1966).

16. S. A. Fedulov, P. B. Ladyzhenskii and Yu. N. Venevtsev, Soviet Phys. - Crystallography 9, 428 (1965).

17. J. Smit and H. P. J. Wijn, Ferrites (John Wiley, 1959), pp. 157-158.

18. H. Tamura et al., Japan. J. Appl. Phys. 4, 621 (1965).

19. B. M. Wanklyn, J. Crystal Growth 5, 323 (1969).

20. S. K. Kurtz and T. T. Perry, J. Appl. Phys. 39, 3798 (1968).

21. K. A. Valiev et al., JETP Letters 12, 12 (1970); Sov. Phys. - Solid State 13, 342 (1971).

22. G. Andersson, Acta Chem. Scand. 10, 623 (1956).

23. J. C. Nickerson et al., Phys. Rev. B3, 2030 (1971).

24. M. B. Maple and D. Wohlleben, Phys. Rev. Letters 27, 511 (1971).

25. R. L. Cohen, M. Eibschutz, and K. W. West, Phys. Rev. Letters 24, 383 (1970).

26. A. Menth, E. Buehler, and T. H. Geballe, Phys. Rev. Letters 22, 295 (1969).

27. E. E. Vainshtein, S. M. Blokhin, and Yu. B. Paderno, Sov. Phys. - Solid State 6, 2318 (1965).

28. A. Jayaraman et al., Phys. Rev. Letters 25, 1430 (1970).

29. A. Jayaraman et al., Phys. Rev. Letters 25, 368 (1970).

30. E. Bucher et al., J. Applied Phys. 42, 1741 (1971).

31. F. Mehran et al., Phys. Rev. Letters 27, 1368 (1971).

32. J. F. Miller et al., Air Force Avionics Lab. Rept. ALTDR 64-239, Contract AF33(657)-10687 (Battelle, (1964)).

33. J. H. Van Vleck, The Theory of Electric and Magnetic Susceptibilities, (Oxford University Press, London, 1932), pp. 245ff.

34. A. Dupont, J. Opt. Soc. of America 57, 867 (1967).

35. W. E. Bron and W. R. Heller, Phys. Rev. 136, A1433 (1964).

36. R. J. Birgeneau et al., Phys. Rev. B5, 3412 (1972).

37. W. P. Wolf and J. H. Van Vleck, Phys. Rev. 118, 1490 (1960).

38. E. D. Jones, Phys. Rev. 180, 455 (1969), and references contained therein.

39. A. J. Darnell et al., Atomic International Report AI-70-81 (Nov., 1970) on Contract DAHC15-70-C-0145, ARPA Order 1518.